Universidad de Valladolid

ESCUELA DE INGENIERÍAS INDUSTRIALES

UNIVERSIDAD DE VALLADOLID

ESCUELA DE INGENIERIAS INDUSTRIALES

Máster en Ingeniería Química

Estudio cinético sobre la desulfuración y la desnitrogenación de destilados de petróleo medios

Autor:

García Riesco, Luis Miguel

RIB: Bolado Rodriguez, Silvia

Universiteit Gent

Valladolid, Mayo 2021

TFM REALIZADO EN PROGRAMA DE INTERCAMBIO

TÍTULO:	A kinetic study on the desulfurization and denitrogenation of medium oil cuts
ALUMNO:	Luis Miguel García Riesco
FECHA:	03/05/2021
CENTRO:	Laboratory for Chemical Technology (LCT)
UNIVERSIDAD:	Ghent University
TUTORES:	Joris W. Thybaut, Kevin Van Geem

Resumen

El hidrotratamiento de dos fracciones medias de petróleo (Diesel y Coker Gasoil) se analizó mediante simulación utilizando un modelo de reactor flujo pistón y diferentes enfoques cinéticos. El estudio se centró en las reacciones de hidrodesulfuración (HDS) e hidrodesnitrogenación (HDN).

Las materias primas se procesaron en un rango de temperaturas de 335 a 365ºC, la presión de operación varió entre 3.5 y 5.1 MPa y el LHSV se ajusto entre 0.7 y 3.5 h-1.

Se evaluó la precisión de los distintos enfoques, así como el significado cualitativo de los parámetros cinéticos. Se encontró que uno de los modelos estudiados predijo el 66% de los experimentos en el rango de incertidumbre con un coeficiente de correlación de Pearson de r = 0.941, mientras que el segundo modelo solo alcanzó el 48% de los experimentos en el rango deseado, con un coeficiente de correlación de Pearson de r = 0.789.

Palabras clave

Hidrotratamiento, desulfuración, desnitrogenación, TBR, modelado cinético.

FACULTY OF ENGINEERING AND ARCHITECTURE

A kinetic study on the desulfurization and denitrogenation of medium oil cuts

Luis Miguel García Riesco

Supervisors: Prof. Dr. Ir. Joris W. Thybaut, Prof. Dr. Ir. Kevin Van Geem.
Counsellors: MSc. Ir. César Pernalete

Master's dissertation submitted in order to obtain the academic degree of
Master of Science in Chemical Engineering

Department of Materials, Textiles and Chemical Engineering
Faculty of Engineering and Architecture
Academic year 2020-2021

GHENT UNIVERSITY

LABORATORY FOR CHEMICAL TECHNOLOGY
Technologiepark 125, 9052 Gent, Belgium

Declaration concerning the accessibility of the master thesis

Undersigned,

Luis Miguel García

Graduated from Ghent University, academic year 2020/2021 and is author of the master thesis with title:

A kinetic study on the desulfurization and denitrogenation kinetics of medium oil cuts

19/04/2021

Luis Miguel García

GHENT UNIVERSITY

LCT
DRIVING CHEMICAL TECHNOLOGY

ACKNOWLEDGEMENTS

I would like to start by thanking the Ghent University and the University of Valladolid for allowing me to study at Ghent during this year through an Erasmus scholarship. Specially, I want to say thank you to my personal coach, César Pernalete, who has been my firsthand support and who helped me during the thesis development.

Within the Ghent University, thank you to my supervisors and assistants, who also helped and contributed to this Master thesis. I regret that I did not have the chance to meet them all in person because of Corona pandemic.

Within the University of Valladolid, I must be very grateful with all my teachers who taught me all the knowledge that I have applied in this work, and specially to the responsible tutor of my exchange programme, Silvia Bolado.

Thanks to all the friends that I met through this Erasmus period, people that little by little have become such a second family. I am very glad that I met a lot of people at the UGent accommodation since at least we could have some meals and chats together. Specially to Ana, a wonderful singer and, above all, a very warm friend.

Finally, I really want to thank my family and my friends from Valladolid who supported me and who were every day caring and worrying about me, without them, it would not have been possible for me to do this thesis.

¡Muchas gracias a todos! (Thank you all!)

ABSTRACT

Hydrotreating processes play a vital role in petroleum refineries to meet the increasing demand of fuels and oil fractions and to guarantee the long-term viability of the refining business. Different kinetic approaches have been proposed in the past to model this process, each one with specific advantages in simplicity or accuracy.

The hydrotreating of medium oil cuts was analysed via simulation using a heterogeneous plug-flow reactor model and different kinetic approaches. The study was focused on the hydrodesulfurization (HDS) and hydrodenitrogenation (HDN) reactions.

The dataset comprised two medium oil fractions: diesel fraction (DF) and coker gasoil (CGO). The feeds were processed in a range of temperatures from 335 to 365ºC, the operation pressure varied from 3.5 MPa to 5.1 MPa and the LHSV was set from 0.7 to 3.5 h-1.

The accuracy of the different approaches is assessed as well as the qualitative meaning of the kinetic parameters. It was found that with one of the studied models 66% of the experiments were predicted in the given range of experimental uncertainty, with a Pearson correlation coefficient of the linear regression of the parity plot of r = 0.941, while in the second model only the 47% of the experiments were predicted in the desired range, with a Pearson correlation coefficient of the parity plot of r = 0.789.

Keywords: hydrotreating, desulfurization, denitrogenation, TBR, reactor modelling, kinetic modelling.

A kinetic study on the desulfurization and denitrogenation of medium oil cuts

Luis Miguel García Riesco

Supervisor(s): Joris Thybaut, Kevin Van Geem

Counsellor(s): César Pernalete

Abstract: **Hydrotreating is an essential process to ensure the long-term viability of the refining business. Different kinetic approaches have been proposed in the past to model this process, each one with specific advantages in simplicity or accuracy. The hydrotreating of medium oil cuts was analyzed via simulation using a heterogeneous plug-flow reactor model and different kinetic approaches. The study was focused on the hydrodesulfurization (HDS) and hydrodenitrogenation (HDN) reactions. The dataset comprised two medium oil fractions whose mixtures were hydrotreated at pilot scale using different process conditions. The accuracy of the different approaches is assessed as well as the qualitative meaning of the kinetic parameters. It was found that with one of the studied models 66% of the experiments were predicted in the given range of experimental uncertainty, with a Pearson correlation coefficient of the linear regression of the parity plot of r = 0.941, while in the second model only the 47% of the experiments were predicted in the desired range, with a Pearson correlation coefficient of the regression of the parity plot of r = 0.789.**

Keywords: **hydrotreating, desulfurization, denitrogenation, TBR, reactor modelling, kinetic modelling.**

I. Introduction

The decline of conventional light crude oil reservoirs has created a scenario in which contaminant removal and upgrading heavier crude oil fractions are key operation in the refining industry to ensure the economic viability in the long term [1][2].

Hydrotreating (HDT) is a process of particular interest to the petroleum because it allows to remove contaminants such as sulfur (S) and nitrogen (N), which can cause detrimental effects on catalysts, affect the quality of the finished products and produce undesired by-products that can also affect the integrity of the plant equipment. In general, hydrotreating is applied prior to other catalytic processes such as fluid catalytic cracking and catalytic reforming [3].

The application of HDT prior to hydrocracking (HCK) comprises the hydroconversion, an important process to upgrade medium and heavy distillates. Typically both operations are carried out in two catalytic reactors in series [4] as it is illustrated in Figure 1.

In hydroconversion, a multistage process is normally preferred over a single-stage reactor since using this configuration the heteroatoms removal reactions and the cracking reactions can take place sequentially in different reactors. Thus, the adverse effects of ammonia and nitrogen compounds on the HCK catalyst can be avoided by an intermediate gases' separation stage.

The main types of reaction that takes place in hydrotreating are hydrodesulphurization (HDS), hydrodenitrogenation (HDN), hydrogenation of aromatics (HAD), hydrodeoxygenation (HDO), olefin saturation and hydrodemetallization (HDM).

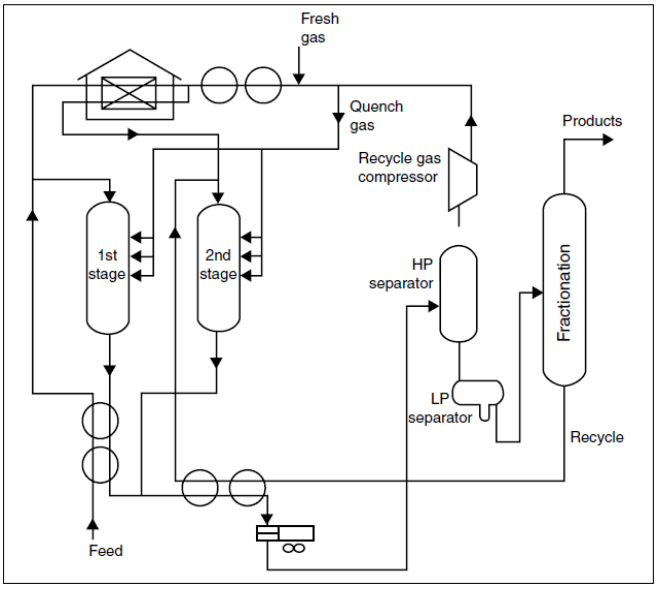

Figure 1. A two stage hydroprocessing unit [5].

The underlying kinetics that takes place in hydrotreating has been extensively studied in the past using different approaches. In the next section, the main types of approaches that have been proposed to model the hydrotreating process, in specific HDS and HDN, will be described. However, the convenience of each approach seems to be strongly dependent on the specific studied case.

The objective of the present work is to investigate via simulation the underlying kinetics of the HDS and HDN in the hydrotreating of different medium oil fractions at pilot scale. The studied Dataset includes variations in different process conditions as well as feed composition. For this purpose, a reactor model is implemented using different kinetic approaches, whose performance is compared in terms of accuracy and generalization capability.

II. Theoretical Background

A. Process description

Hydrotreating starts with the feedstock being is mixed with hydrogen, preheated in a fired heater up to 300 – 450ºC and

L.M. García is with the Chemical Engineering Department, Ghent University (UGent), Gent, Belgium. E-mail: LuisMiguel.Garcia@UGent.be .

later fed to a fixed-bed catalytic reactor under pressures even higher than 100 bar. The catalysts used for HDT are typically made of nickel-molybdenum (Ni-Mo) or cobalt-molybdenum (Co-Mo) supported on alumina, often doped by fluorine or phosphorus [6].

In the reactor, the sulfur atoms present as heteroatoms in the feedstock are converted to hydrogen sulfide, and the corresponding nitrogen atoms are converted to ammonia. The reaction products leave the reactor and, after cooled, they enter a liquid/gas separator. The hydrogen-rich gas from the high-pressure separation is recycled and combined with the feedstock, and the low-pressure gas stream rich in light hydrocarbons, H_2S and NH_3 is sent to a gas-treating unit where sour gases are removed. After this process, the gas stream becomes clean and suitable as fuel for the refinery furnaces [3].

The main hydrotreating operating variables are reactor bed temperature, H_2 partial pressure, H_2/oil ratio and liquid hourly space velocity (LHSV). The values of these operating variables depend on the quality of the feedstock and the desired product specification.

B. Hydrodenitrogenation

The total nitrogen content in medium/heavy fractions is typically lower than 4000 wt ppm [7]. Organonitrogen compounds are undesired in the refining process because, even at low levels, cause an inhibition effect in HCK catalysts. In HDN, the direct breakage of C-N bond in heterocyclic aromatic molecules if very unlikely. This reaction is difficult even in exocyclic molecules such as aniline, for which hydrogenation to cyclohexylamine precedes C-N bond breaking [8].

Some HDN kinetic models lump all basic-nitrogen compounds and, in another lump, all non-basic nitrogen compounds. It is well-known that the non-basics are first hydrogenated to basic compounds [9][10] before reactions to eliminate the nitrogen atom from the molecule occur.

The pyridine hydrodenitrogenation has been extensively studied in previous works by Raghuveer et al. [11][12] using elementary step kinetics. In this work, nitrogen is predominantly eliminated via a H_2S enhanced substitution mechanism.

More complex nitrogen molecules, such as quinoline, are expected to follow a similar reaction pathway to that of pyridine. Among basic heterocyclic N-containing compounds, quinoline is a widely used as model molecule in HDN studies. The mechanism for quinoline HDN has been previously studied [13][14] and includes successive hydrogenation of benzenic rings, hydrogenation of aromatic heterocyclic rings and C-N bond cleavage.

Girgis and Gates' work [15] thoroughly reviewed the HDN and HDS of the most relevant nitrogen and sulfur compounds including data characterizing thermodynamics, .reactivities, reaction networks and kinetic expressions. This work best summarizes the main HDT reactions and suggests the need of modelling complex industrial feeds and mixtures.

C. Hydrodesulfurization

Sulfur content of medium distillates generally falls in the range of 0.5-2 wt% [16]. In general, the distribution of sulfur in oil fractions is such that the proportion of sulfur increases along with the boiling point of the distillate fraction [17].

Sulfur compounds in middle distillates may be classified into groups by compound types such as mercaptans, sulfides and aromatic sulfur compounds such as thiophenes, benzothiophenes, dibenzothiophenes and the corresponding alkyl substituents of these compounds [16].

Due to the large number of sulfur compounds in the different oil fractions, as well as the existing limitations for their identification and measurement, could be challenging to model all hydrodesulfurization reactions individually. For that reason, in some kinetic desulfurization studies, all sulfur compounds are grouped as a single lump and considered as a single global reaction [10][18].

Generally acyclic sulfur compounds such as thiols and disulfides are highly reactive and can be removed under very mild conditions. Since the reactivity of mercaptans and sulfides is similar, in some models do not explicitly differentiate these compounds and lump them into mercaptans [19]. The desulfurization of mercaptan is a reversible reaction, where the olefin formed can react with H_2S reverting back to the mercaptan [19].

Other works modelled hydrotreating processes of medium distillates such as diesel using an integrated design approach, which also considers the capital and operating costs associated [15, 18].

Detailed kinetic equations for the conversion of thiophene, benzothiophene and dibenzothiophene has been extensively investigated in the past [21][22][23]. The existence of two different active sites, σ-sites for hydrogenolysis reactions, and τ-sites for hydrogenation was one of the main conclusions in those researches. In addition, the competitive adsorption of H_2 and H_2S is a generally accepted phenomenon.

Owing to the high boiling point of the medium/heavy distillates, it is possible to find more complex molecules in the feed than the ones mentioned such as 4,6-dimethyldibenzothiophene (4,6-DM-DBT). In comparison with other components, 4,6-DM-DBT has proved to be a molecule with low reactivity due to the steric hindrance brought by the alkyl groups in 4,6-DM-DBT [24].

One big challenge when modelling the hydrotreatment of oil cuts is the molecular diversity of hydrocarbons, organosulfur, organonitrogen and other molecules with heteroatoms existing in the feedstock. An interesting method used when modelling petroleum fractions is the lumping approach, which consists of regrouping chemical compounds by similar properties in clusters called lumps.

Due to the multicomponent characteristic of the lumps, the reactions pathways are generally global, with no intermediate species, and the kinetic rate equations are often pseudo-order reactions or Langmuir-Hinshelwood type expressions [25].

D. Hydrotreating reactor

Hydrotreating units for light feeds are carried out in two-phase fixed-bed reactors. However, when the boiling point of the feed increases, three phases will be found: hydrogen, a liquid-vapor mixture of the partially vaporized feed, and the solid catalyst. This reaction system is called trickle-bed reactor (TBR), which is referenced in the literature as a reactor in which a liquid phase and a gas phase flow concurrently downward through a fixed-bed of catalyst particles while reactions occur [26].

The kinetic modelling of a TBR is usually based on the two-film theory where the resistance to mass transfer in a given turbulent fluid phase is present in a thin layer adjacent to the interface that is called a film [27]. In a TBR, the gas and

liquid reactants are effectively contacted over the surface of a solid catalyst in a co-current down-flow mode.

III. METHODOLOGY

The applied methodology consisted in four stages: i) Dataset qualitative analysis, ii) Reactor and kinetic model formulation, iii) Kinetic parameter determination and iv) Model assessment. Once the model is evaluated the method considers adjustments over the original model formulation in an iterative approach.

A. *Data set analysis*

The experimental determination of the studied Dataset was performed by hydrotreating in a pilot-plant rig mixture of two different medium oil fractions that are labeled as Diesel fraction (DF) and coker gasoil (CGO). Table 1 shows the sulfur and nitrogen content of each feed, as well as their mixture proportions. The processed feeds are DF, DF+15%CGO and DF+30%CGO.

Table 1. Feed sulfur and nitrogen content.

Feed	Total sulfur, ppm	Total nitrogen, ppm	Mercaptans ppm	Thiophenes, ppm	DBT, ppm	Alkyl DBT, ppm
DF	20620	186	10289	9107	948	277
CGO	22860	766	19776	2822	206	56
DF+15% CGO	20956	254	11712	8164	837	244
DF+30% CGO	21292	360	13135	7222	725	210

The feeds were processed in a range of temperatures from 335 to 365ºC. The operation pressure varied from 3.5 MPa to 5.1 MPa and the LHSV was set from 0.7 to 3.5 h^{-1}. 53 experimental points were produced in total.

B. *Model formulation*

A steady state reactor model was formulated according to the following considerations:

- Constant gas and liquid velocities across the reactor
- No radial concentration gradients
- Mass transfer effects described by the two-film theory
- **C**atalyst surface is completely covered by a liquid film
- Constant catalyst activity in time
- No vaporization/condensation of S and N compounds
- All reaction take place in liquid phase
- Reaction rate constants described by Arrhenius law
- Adsorption constants described by Van't Hoff equation

The reactor is integrated along its length (z). The mass-balance equations for the gas compounds can be described as:

$$\frac{u_G}{RT}\frac{dP_i^G}{dz} + k_i^G a_L\left(\frac{P_i^G}{H_i} - C_i^L\right) = 0 \quad (1)$$

The mass-balance equation for the organic nitrogen and sulfur compounds in the liquid phase is:

$$u_L\frac{dC_i^L}{dz} + k_i^S a_S\left(C_i^L - C_i^S\right) = 0 \quad (2)$$

Based on the model, the driving force in the liquid-solid interface can be described as:

$$k_i^S a_S\left(C_i^L - C_i^S\right) = -v_i\, r = -v_i\, \rho_B\, r_j \quad (3)$$

A global energy balance can be obtained with the addition of both gas and liquid contributions:

$$\frac{dT}{dz} = \sum[(-\Delta H_{R_i})(r_i)] \cdot \frac{\epsilon_L}{u_G\,\rho_G\,c_{P_G}\epsilon_G + u_L\,\rho_L\,c_{P_L}\epsilon_L} \quad (4)$$

The mass balance equations assume that the gas-liquid equilibrium for this mixture can be described by the Henry's law. The henry coefficient H_i can be obtained from solubility coefficients λ_i:

$$H_i = \frac{v_N}{\lambda_i \cdot \rho_L} \quad (5)$$

The gas-liquid mass transfer coefficient is a function of the liquid superficial velocity, G_L. For its determination it is possible to use a correlation from the literature [28]:

$$\frac{k_i^L \cdot a_L}{D_i^L} = \alpha_1 \cdot \left(\frac{G_L}{\mu_L}\right)^{\alpha_2} \cdot \left(\frac{\mu_L}{\rho_L \cdot D_i^L}\right)^{1/2} \quad (6)$$

Two different kinetic models were formulated and, in both cases, the sulfur compounds were classified in 4 lumps: mercaptans, thiophenes, dibenzothiophenes (DBT) and alkyl dibenzothiophenes (alkyl DBT). Model A classifies nitrogen compounds in two lumps, basic and non-basic, while in Model B nitrogen compounds are considered as a single lump.

1) *Model A. High order kinetic models*

The kinetic expression for the nitrogen lumps was assumed as a first order reaction rate depending on both reactants (H_2 and 'i' nitrogen compound). Mercaptans are highly reactive, by which the same type of expression was applied to model this reaction as follows:

$$r_i = k_i\, C_i\, C_{H_2} \quad (7)$$

The kinetic expression assumes competitive adsorption on the same catalytic sites between the reactant H_2, H_2S and the lump 'i' (thiophenes, DBT and alkyl DBT):

$$r_i = \frac{k_i K_i (C_i)^p K_{H_2} (C_{H_2})^q}{\left(1 + K_{H_2S} C_{H_2S} + K_{H_2} C_{H_2} + K_i C_i\right)^3} \quad (8)$$

Where p and q are the reaction order of the reactant i and H_2 respectively. K_i is the equilibrium adsorption constant of component i, which was calculated via Van't Hoff equation:

$$K_i = e^{\frac{\Delta S_{ads\,i}}{R}} \cdot e^{-\frac{\Delta H_{ads\,i}}{RT}} = B_i \cdot e^{-\frac{\Delta H_{ads\,i}}{RT}} \quad (9)$$

Reaction rate constants were calculated by the Arrhenius law:

$$k = A \cdot e^{-\frac{E_a}{RT}} \quad (10)$$

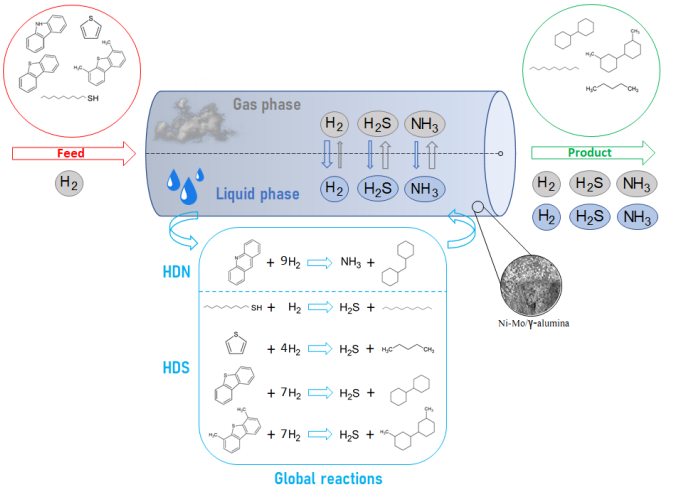

Figure 2. Model description with global hydrotreating reactions.

In Figure 2 a schematic description of the reactor model and the considered hydrotreating reactions that occur are illustrated.

2) Model B. Two active sites for HDS

Two catalytic active sites were considered in this second kinetic model: σ-sites for hydrogenolysis reactions and τ-sites for hydrogenation reactions.

The total nitrogen content was modelled in one lump with acridine as reference molecule. The kinetic expression was proposed following a law of mass action approach:

$$r_{HDN} = k_{HDN}\, C_N^{1.5}\, C_{H_2}^{1.5} \tag{11}$$

The mercaptans HDS reaction was described as a reversible reaction, as depicted graphically in Figure 3. According to Ghosh et al. [19] the forward reaction dominates for the most part.

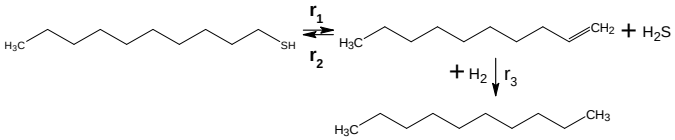

Figure 3. Decanethiol HDS reaction network

$$r_1 = k_1\, C_{Merc} \quad r_2 = k_3\, C_{Olef}\, C_{H_2S} \quad r_3 = k_2\, C_{Olef} \tag{12}$$

Thiophenes HDS reactions were modelled with an intermediate step where the thiophene is hydrogenated to tetrahydrothiophene (TT), as shown in Figure 4. Hydrogenolysis and hydrogenation were assumed to occur in different catalytic sites and, therefore, two independent reaction rates were required [15][21].

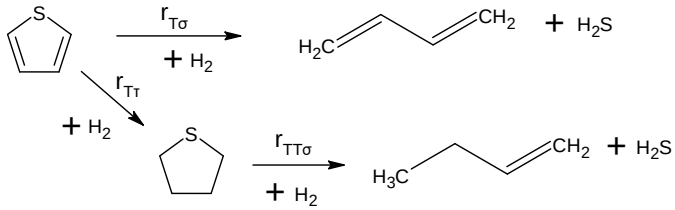

Figure 4. Thiophene HDS reaction network.

$$r_{T\sigma} = \frac{k_{T\sigma}\, C_T\, C_{H_2}}{1 + K_T C_T + K_{H_2S} C_{H_2S}} \quad r_{T\tau} = k_{T\tau}\, C_T\, C_{H_2} \quad r_{TT\sigma} = \frac{k_{T\sigma}\, C_{TT}\, C_{H_2}}{1 + K_T C_T + K_{H_2S} C_{H_2S}} \tag{13}$$

Dibenzothiophenes were modelled following the same reaction scheme, with THDBT as intermediate reaction specie as described graphically in Figure 5. Kinetic expressions for hydrogenolysis and hydrogenation were taken from previous works [29].

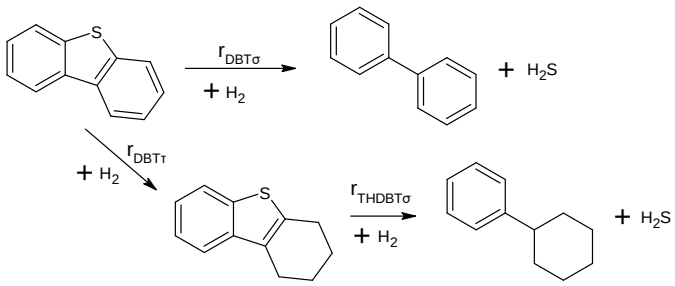

Figure 5. Dibenzothiophene HDS reaction network.

$$r_{DBT\sigma} = \frac{k_{DBT\sigma} K_{DBT\sigma} K_{H_2\sigma} C_{DBT} C_{H_2}}{(1 + K_{DBT\sigma} C_{DBT} + \sqrt{K_{H_2\sigma} C_{H_2}} + K_{H_2S} \frac{C_{H_2S}}{C_{H_2}})} \quad r_{DBT\tau} = \frac{k_{DBT\tau} K_{DBT\tau} C_{DBT} C_{H_2}}{(1 + K_{DBT\tau} C_{DBT})^3} \tag{14}$$

Alkyl dibenzothiophenes were modelled using the same kinetic expressions as the case for dibenzothiophenes, but in this case using 4,6-DMDBT as a reference molecule.

C. Parameter determination

Kinetic parameters are determined by solving the following optimization problem:

$$\min_{\lambda \in X} \sum_{i=1}^{N_{Lumps}} \sum_{j=1}^{N_{Experiments}} \left[C_{exp}(i,j) - C_{sim}(i,j)\right]^2 \tag{15}$$

As described in Eq. 14, the objective function was posed as the sum of squared errors (SSE) between the experimental and simulated concentrations of nitrogen and sulfur species in the product for each of the studied experiments.

D. Model assessment and comparison

In order to evaluate the accuracy of the models the following analysis were carried out:

1) Statistical values. Includes the variance, standard deviation and correlation coefficient of simulated values.
2) Parity diagram.
3) Residual analysis.

IV. RESULTS

A. Data set analysis

From Table 1 it can be observed that CGO has a higher content in both nitrogen and sulfur compounds than DF. Mercaptans and thiophenes are the compound lumps with more sulfur content in the feedstocks, representing about 90% of the total content.

The HDS (left) and HDN (right) conversions for each processed feed is graphically described in Figures 6, 7 and 8 respectively. For each condition of reaction temperature, pressure and LHSV the conversion is illustrated in a color/size scale.

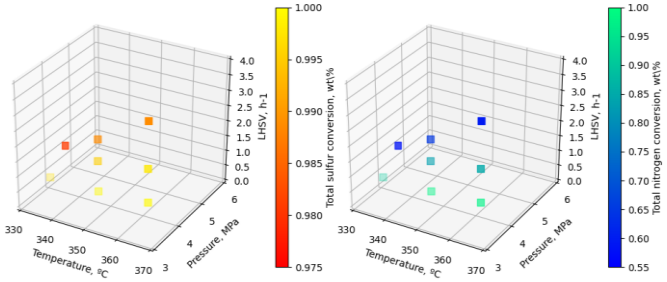

Figure 6. Conversions of DF hydrotreating at different process conditions

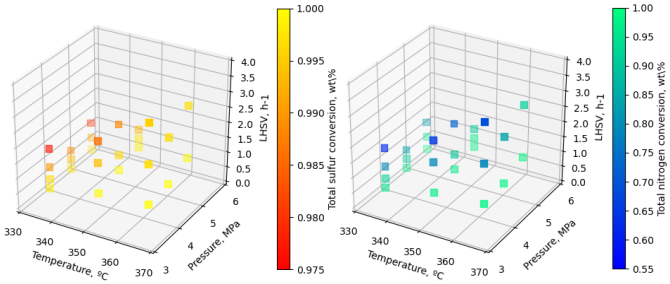

Figure 7. Conversions of DF + 15% CGO hydrotreating at different process conditions

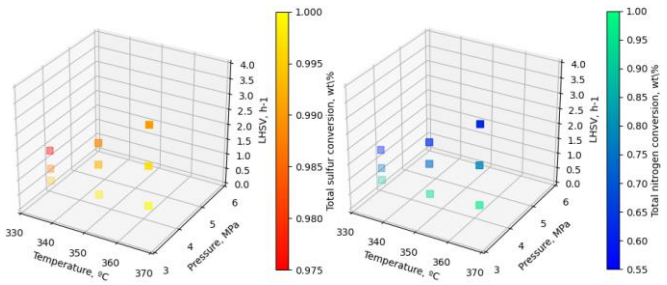

Figure 8. Conversions of DF + 30% CGO hydrotreating at different process conditions.

From these figures some qualitative conclusions can be drawn. On the one hand, the highest conversions are achieved when working at the highest temperatures and the lowest LHSV, as expected. The temperature effect on the conversion predominates over the rest of the conditions. It is important to remark that at low LHSV just high conversions are obtained, which indicate a strong influence of this variable on the conversion.

The experiments were carried out at different operating conditions. Some of the experiments were repeated using the same conditions and different values in the product composition were obtained. Table 2 shows the standard deviations in the results of these experiments.

Table 2. Standard deviations in repeated experiments.

Total S, ppm	Total N, ppm	Mercaptans, ppm	Thiophenes, ppm	DBT, ppm	Alkyl DBT, ppm
42.69	10.72	8.61	26.35	7.63	7.72

B. Kinetic model A

A comparison of experimental and simulated concentrations described by model A is shown in Figure 9.

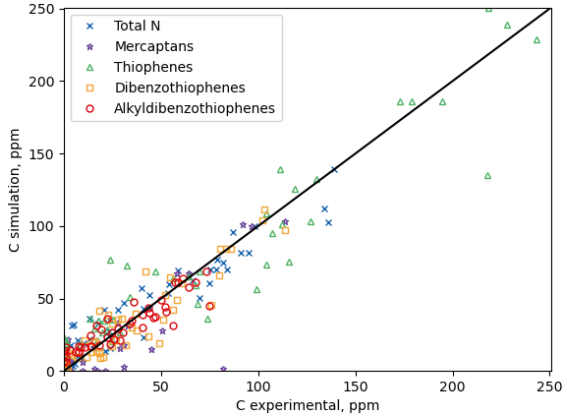

Figure 9. Comparison between experimental and simulated concentrations by model A.

The Pearson correlation coefficient for the parity plot of all predictions is r = 0.941. In the simulation 66% of the experimental points lie in the range covered by the uncertainty given by ± the range [-σ, +σ] where σ is the standard deviation calculated from the results of repeated experiments. The lumps whose conversion is better described by the model is thiophenes, with 81% of the experimental points simulated into the range of experimental uncertainty.

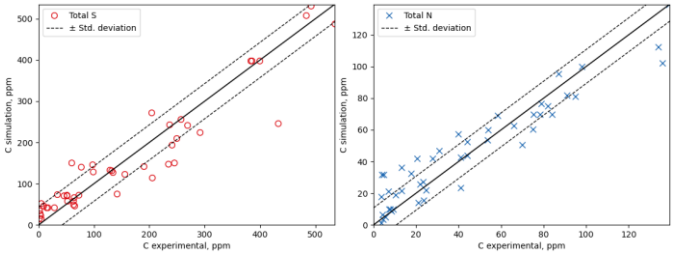

Figure 10. Experimental and simulated points of total sulfur and total nitrogen.

Figure 10 illustrates the simulated vs experimental points of total sulfur and total nitrogen concentrations. In this simulation, 70% of the total sulfur points lie inside the given uncertainty, whereas in case of nitrogen 64% of the points were properly predicted.

Table 3 shows the values for kinetic and adsorption parameter determined by the parameter optimization procedure. The table also includes the apparent reaction constants 'k_{app}' at 350ºC. In general, the value for activation energy of all compounds is in the order of 10 kJ/mol and 100 kJ/mol as reported in other works. Values for k_{app} for sulfur compounds with the same kinetic expression (thiophenes, DBT and alkyl DBT) adopted similar values with a slightly higher value for DBT. This fact could reflect the ability of the catalyst to equally promote the reaction of all thiophenic compounds. Even with similar k_{app} to thiophenes and DBT, the adsorption pre-exponential constant for alkyl DBT was found very low, which is attributed to the low probability of this compounds to be adsorbed on the catalyst surface due to its steric hindrance.

Table 3. Kinetic and adsorption parameter values.

	A	Ea, J/mol	B	Hads, J/mol	k_{app} (350ºC)
Total N	1.51E+17	1.24E+05	-	-	5.83E+06
Mercaptans	9.58E+17	1.52E+05	-	-	1.57E+05
Thiophenes	2.95E+15	8.35E+04	5.41E+03	5.90E+04	1.80E+07
DBT	2.52E+17	1.12E+05	2.75E+03	4.86E+04	2.34E+07
Alkyl DBT	6.57E+21	1.05E+05	1.83E-06	9.69E+01	1.75E+07
H_2	-	-	1.11E+03	6.11E+04	-
SH_2	-	-	5.46E+04	6.34E+04	-

The determined reaction orders were p = 1.51 (for sulfur compound) and q = 0.41 (for H_2). Similar reaction orders were found for hydrogen in previous HDS researches [10].

In Figure 11, the residual graphs of total nitrogen are illustrated against the main operational variables. It can be observed that the residual values seem to be slightly correlated with the LHSV variable. A similar behavior was observed when plotting the total sulfur residuals. This fact can explain that the strong effect of the LHSV on the conversions was not accurately predicted by the model as for the rest of the operating variables.

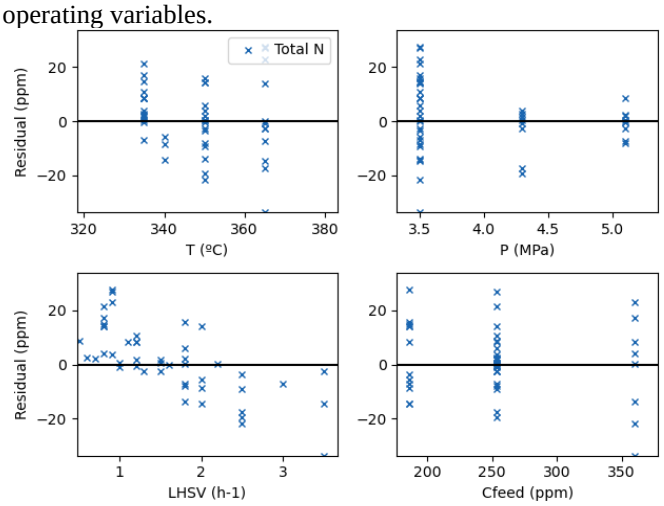

Figure 11. Residual values of total nitrogen concentrations in the product.

C. Kinetic model B

A comparison of experimental and simulated concentrations described by model B is shown in Figure 12.

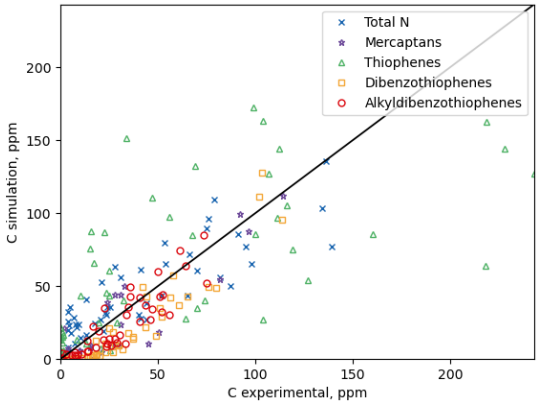

Figure 12. Comparison between experimental and simulated concentrations by model B.

The Pearson correlation coefficient for this model is r = 0.789. In this simulation only 47% of the points lie in the range of the experimental uncertainty. The lumps for which the conversion was better described was mercaptans model where 72% of the experimental points were predicted in the range of the considered experimental uncertainty. In this simulation, 68% of the total sulfur points lied inside the given uncertainty, whereas in case of nitrogen only 38% of the points were properly predicted.

Comparing the results obtained in this model with those obtained in the first model, it can be concluded that better predictions in both the HDS and HDN conversions can be obtained using the kinetics described in model A.

CONCLUSIONS

Two different kinetic approaches were proposed to model the hydrotreating of medium oil cuts. The first model was based on global kinetics for sulfur and nitrogen compounds. The second model was based on a more detailed kinetic formulation that considers different active sites for the hydrogenolysis and the hydrogenation reaction of sulfur compounds, reversibility in the mercaptans reaction and higher order for nitrogen reactions. Better predictions were obtained with the first model in terms of the number of the Pearson correlation coefficient of the regression line in the global parity plot and the number of points predicted by the models in the expected uncertainty range. In general, the apparent reaction rates for all the lumps were found reasonable considering the expected reactivity of the molecule. A strong correlation with LHSV was observed in the residuals of most of the variables which indicate a strong influence of this variable on the final conversion that must be better addressed by the model.

REFERENCES

[1] M. Mohammadpoor and F. Torabi, “Big Data analytics in oil and gas industry: An emerging trend,” *Petroleum*, 2018, doi: https://doi.org/10.1016/j.petlm.2018.11.001.

[2] E. Iplik, I. Aslanidou, and K. Kyprianidis, “Hydrocracking: A Perspective towards Digitalization,” *Sustainability*, vol. 12, no. 17, p. 7058, Aug. 2020, doi: 10.3390/su12177058.

[3] N. P. Cheremisinoff and P. Rosenfeld, “Chapter 1 - The petroleum industry,” N. P. Cheremisinoff and P. B. T.-H. of P. P. and C. P.-B. P. in T. P. I. Rosenfeld, Eds. Oxford: William Andrew Publishing, 2009, pp. 1–97.

[4] N. Bergvall, L. Sandström, F. Weiland, and O. G. W. Öhrman, “Corefining of Fast Pyrolysis Bio-Oil with Vacuum Residue and Vacuum Gas Oil in a Continuous Slurry Hydrocracking Process,” *Energy & Fuels*, vol. 34, no. 7, pp. 8452–8465, Jul. 2020, doi: 10.1021/acs.energyfuels.0c01322.

[5] X. Liang, Y. Liu, and L. Kang, “Retrofit and optimisation for a vacuum gas oil hydrotreating system based on exergy load distribution analysis,” *Int. J. Exergy*, vol. 21, p. 347, Jan. 2016, doi: 10.1504/IJEX.2016.080066.

[6] S. Vedachalam, A. Dalai, and J. Adjaye, “The effect of phosphorus on hydrotreating property of NiMo/γ-Al 2O 3 nitride catalyst,” *Appl. Catal. A-general - APPL CATAL A-GEN*, vol. 335, pp. 204–210, Feb. 2008, doi: 10.1016/j.apcata.2007.11.024.

[7] N. Charon-Revellin, H. Dulot, C. Lopez-Garcia, and J. Jose, “Kinetic Modeling of Vacuum Gas Oil Hydrotreatment using a Molecular Reconstruction Approach,” *Oil Gas Sci. Technol.*, vol. 66, pp. 479–490, May 2010, doi: 10.2516/ogst/2010005.

[8] R. Prins, M. Egorova, A. Röthlisberger, Y. Zhao, N. Sivasankar, and P. Kukula, “Mechanisms of hydrodesulfurization and hydrodenitrogenation,” *Catal. Today*, vol. 111, no. 1, pp. 84–93, 2006, doi: https://doi.org/10.1016/j.cattod.2005.10.008.

[9] S. K. Bej, A. K. Dalai, and J. Adjaye, “Comparison of Hydrodenitrogenation of Basic and Nonbasic Nitrogen Compounds Present in Oil Sands Derived Heavy Gas Oil,” *Energy & Fuels*, vol. 15, no. 2, pp. 377–383, Mar. 2001, doi: 10.1021/ef0001484.

[10] M. A. Rodríguez and J. Ancheyta, “Modeling of Hydrodesulfurization (HDS), Hydrodenitrogenation (HDN), and the Hydrogenation of Aromatics (HDA) in a Vacuum Gas Oil Hydrotreater,” *Energy & Fuels*, vol. 18, no. 3, pp. 789–794, May 2004, doi: 10.1021/ef030172s.

[11] C. S. Raghuveer, “Hydrodenitrogenation kinetics according to single-event methodology,” 2016.

[12] C. S. Raghuveer, J. W. Thybaut, R. De Bruycker, K. Metaxas, T. Bera, and G. B. Marin, “Pyridine hydrodenitrogenation over industrial NiMo/γ-Al2O3 catalyst: Application of gas phase kinetic models to liquid phase reactions,” *Fuel*, vol. 125, pp. 206–218, 2014, doi: https://doi.org/10.1016/j.fuel.2014.02.017.

[13] M.-T. Nguyen, M. Tayakout-Fayolle, F. Chainet, G. D. Pirngruber, and C. Geantet, “Use of kinetic modeling for investigating support acidity effects of NiMo sulfide catalysts on quinoline hydrodenitrogenation,” *Appl. Catal. A Gen.*, vol. 530, pp. 132–144, 2017, doi: https://doi.org/10.1016/j.apcata.2016.11.015.

[14] M.-T. Nguyen, M. Tayakout-Fayolle, G. D. Pirngruber, F. Chainet, and C. Geantet, “Kinetic Modeling of Quinoline Hydrodenitrogenation over a NiMo(P)/Al2O3 Catalyst in a Batch Reactor,” *Ind. Eng. Chem. Res.*, vol. 54, no. 38, pp. 9278–9288, Sep. 2015, doi: 10.1021/acs.iecr.5b02175.

[15] M. J. Girgis and B. C. Gates, “Reactivities, reaction networks, and kinetics in high-pressure catalytic hydroprocessing,” *Ind. Eng. Chem. Res.*, vol. 30, no. 9, pp. 2021–2058, Sep. 1991, doi: 10.1021/ie00057a001.

[16] M. I. Ahmad, “Integrated and Multi-Period design of Diesel Hydrotreating Process,” 2009.

[17] M. J. Grossman, M. K. Lee, R. C. Prince, K. K. Garrett, G. N. George, and I. J. Pickering, “Microbial desulfurization of a crude oil middle-distillate fraction: analysis of the extent of sulfur removal and the effect of removal on remaining sulfur,” *Appl. Environ. Microbiol.*, vol. 65, no. 1, pp. 181–188, Jan. 1999, doi: 10.1128/AEM.65.1.181-188.1999.

[18] H. Korsten and U. Hoffmann, “Three-phase reactor model for hydrotreating in pilot trickle-bed reactors,” *AIChE J.*, vol. 42, no. 5, pp. 1350–1360, May 1996, doi: 10.1002/aic.690420515.

[19] P. Ghosh, A. T. Andrews, R. J. Quann, and T. R. Halbert, “Detailed Kinetic Model for the Hydro-desulfurization of FCC Naphtha,” *Energy & Fuels*, vol. 23, no. 12, pp. 5743–5759, Dec. 2009, doi: 10.1021/ef900632v.

[20] M. I. Ahmad, N. Zhang, and M. Jobson, “Integrated design of diesel hydrotreating processes,” *Chem. Eng. Res. Des.*, vol. 89, no. 7, pp. 1025–1036, 2011, doi: https://doi.org/10.1016/j.cherd.2010.11.021.

[21] I. A. Van Parijs and G. F. Froment, “Kinetics of hydrodesulfurization on a cobalt-molybdenum/.gamma.-alumina catalyst. 1. Kinetics of the hydrogenolysis of thiophene,” *Ind. Eng. Chem. Prod. Res. Dev.*, vol. 25, no. 3, pp. 431–436, Sep. 1986, doi: 10.1021/i300023a011.

[22] I. A. Van Parijs, L. H. Hosten, and G. F. Froment, “Kinetics of the hydrodesulfurization on a cobalt-molybdenum/.gamma.-alumina catalyst. 2. Kinetics of the hydrogenolysis of benzothiophene,” *Ind. Eng. Chem. Prod. Res. Dev.*, vol. 25, no. 3, pp. 437–443, Sep. 1986, doi: 10.1021/i300023a012.

[23] D. H. Broderick and B. Gates, “Hydrogenolysis and hydrogenation of dibenzothiophene catalyzed by sulfided Coo_MoO32_Al2O3: The reaction kinetics,” *Aiche J.*, vol. 27, pp. 663–673, 1981.

[24] F. Richard, T. Boita, and G. Pérot, “Reaction mechanism of 4,6-dimethyldibenzothiophene desulfurization over sulfided NiMoP/Al2O3-zeolite catalysts,” *Appl. Catal. A Gen.*, vol. 320, pp. 69–79, 2007, doi: https://doi.org/10.1016/j.apcata.2006.12.014.

[25] L. de Oliveira, D. Hudebine, D. Guillaume, and J. Verstraete, “A Review of Kinetic Modeling Methodologies for Complex Processes,” *Oil Gas Sci. Technol.*, vol. 71, p. 45, May 2016, doi: 10.2516/ogst/2016011.

[26] M. Bhaskar, G. Valavarasu, B. Sairam, K. S. Balaraman, and K. Balu, “Three-Phase Reactor Model to Simulate the Performance of Pilot-Plant and Industrial Trickle-Bed Reactors Sustaining Hydrotreating Reactions,” *Ind. Eng. Chem. Res.*, vol. 43, no. 21, pp. 6654–6669, Oct. 2004, doi: 10.1021/ie049642b.

[27] Z. Chen *et al.*, “Molecular-level kinetic modelling of fluid catalytic cracking slurry oil hydrotreating,” *Chem. Eng. Sci.*, vol. 195, pp. 619–630, 2019, doi: https://doi.org/10.1016/j.ces.2018.10.007.

[28] S. Goto and J. M. Smith, “Trickle-bed reactor performance. Part I. Holdup and mass transfer effects,” *AIChE J.*, vol. 21, no. 4, pp. 706–713, Jul. 1975, doi: https://doi.org/10.1002/aic.690210410.

[29] G. F. Froment, G. A. Depauw, and V. Vanrysselberghe, “Kinetic Modeling and Reactor Simulation in Hydrodesulfurization of Oil Fractions,” *Ind. Eng. Chem. Res.*, vol. 33, no. 12, pp. 2975–2988, Dec. 1994, doi: 10.1021/ie00036a012.

Table of contents

LIST OF FIGURES

LIST OF TABLES

Nomenclature

Roman symbols:

A_0	Pre-exponential Arrhenius factor.
a	Parameter for the liquid viscosity calculation.
a_L	Specific surface area, gas-liquid interface.
a_S	Specific surface area, gas-solid interface.
B_0	Pre-exponential Van't Hoff factor.
C_i	Molar concentration.
c_P	Specific heat capacity.
D	Reactor diameter.
D^L	Molecular diffusivity.
d_P	Particle diameter.
E_a	Activation energy.
G_L	Liquid superficial velocity.
h	Planck's constant.
H_i	Henry's law coefficient.
H_a	Adsorption enthalpy.
K	Equilibrium adsorption constant.
k	Rate constant.
k_B	Boltzmann's constant.
k_i^S	Liquid-solid mass transfer coefficient.
k_i^L	Liquid-gas mass transfer coefficient.
L	Reactor length.
M	Molecular weight.
n_e	Number of single events.
p_i	Partial pressure.
P	Pressure.
T	Temperature.
T_r	Refrigerant temperature.
R	Universal gas constant.
S	Reactor surface.
SG	Specific gravity.
r_i	Reaction rate.
u_i	Superficial velocity.
U	Overall heat transfer coefficient.
V	Reactor volume.
V_c	Catalyst volume.
v_i	Stoichiometric coefficient/Molar volume.
v_C	Critical specific molar volume.
v_N	Molar gas volume at standard conditions.

w_i	Mass fraction.
X	Conversion.
z	Catalyst bed length.

Subscripts:

0	Initial conditions (reactor length, z = 0).
i	Component or lump index.
N	Nitrogen.
N_B	Basic nitrogen.
N_{NB}	Non-basic nitrogen.
S	Sulfur.

Superscripts:

G	Gas.
L	Liquid.
S	Solid.

Greek symbols:

ΔH_R	Heat of reaction.
$\Delta H^{0,\neq}$	Reaction enthalpy.
$\Delta S^{0,\neq}$	Reaction entropy.
σ	Active site for hydrogenolysis.
$\sigma_{gl,r}$	Global symmetry number of reactant.
$\sigma_{gl,r\neq}$	Global symmetry number of transition state.
α_1	Coefficient 1 related to the geometry of the catalyst particle.
α_2	Coefficient 2 related to the geometry of the catalyst particle.
ϵ_L	Liquid fraction.
ϵ_G	Gas fraction.
ε	Bed void fraction.
λ	Solubility coefficient.
ρ	Density.
ρ_B	Bulk density.
ρ_C	Catalyst density.
ρ_{20}	Density at 20ºC.
τ	Active site for hydrogenation
μ	Dynamic viscosity.

Abbreviations:

AGO	Atmospheric Gas Oil
API	American Petroleum Institute.
CV	Cross-validation.
DBT	Dibenzothiophene
HDA	Hydrodearomatization.
HDM	Hydrodemetallization.
HDN	Hydrodenitrogenation.
HDS	Hydrodesulfurization.
HDO	Hydrodeoxigenation.
HDT	Hydrotreating.
LHSV	Liquid Hourly Space Velocity.
THDBT	Tetrahydrodibenzothiophene
TT	Tetrahydrothiophene
SEMK	Single-Event MicroKinetics.

1. Introduction

Petroleum refining is a complex industry that historically has employed technological developments in simulation, automatization and data analytics for design, operation and optimization activities. In this context, chemical process simulation tools are typically used in refineries to address more efficiently different technical tasks [1].

A typical problem in oil refining is the high variability in the composition of the feedstock, which is highly dependent on the location of the oil field [2]. The decline of conventional light crude oil reservoirs has created a scenario in which contaminant removal and upgrading heavier crude oil fractions are key operations in the refining industry. In the long term, complex refining schemes where different fractions are hydrotreated to remove contaminants and heavier fractions are converted via catalysis, as shown in Figure 1.1, are needed to ensure the operational and economic viability of the refining business.

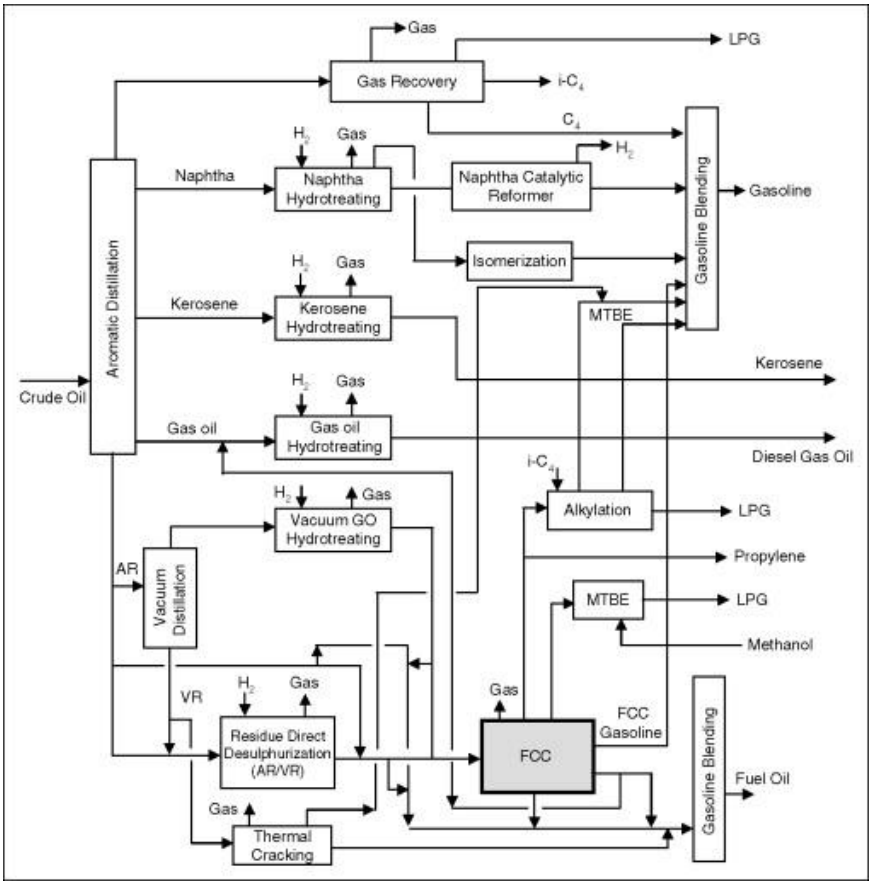

Figure 1.1 Process block diagram in a typical oil refinery [3].

Heavier feedstocks have low API (American Petroleum Institute's) gravity, which is associated with a low hydrogen-to-carbon ratio, high asphaltene and heteroatoms contents such as sulfur (S) and nitrogen (N), and high yield to vacuum distillation residues. Vacuum distillation residues are rich in asphaltenes and metals.

The recent trends in processing heavier crudes with higher sulphur contents and more stringent product specifications for cleaner transportations fuels, such as ultra-low sulphur diesel, are resulting in more efficient processes and more severe operating conditions [4].

One of the most important processes to upgrade medium and heavy oil fractions is hydroconversion. Hydroconversion is an extremely versatile process, capable of treating a wide variety of feedstocks, including light and heavy crude, vacuum gas oil (VGO), coking gas oil (CGO), bitumen, as well as other non-conventional resources such as vegetable oils [5]. This process accounts for 15-17% of the global residue processing capacity.

Hydroconversion of a petroleum fraction comprises Hydrotreatment (HDT) and Hydrocracking (HCK), usually being both operations carried out in two catalytic reactors in series [6]. In general, hydrotreating is applied prior to other catalytic processes such as fluid catalytic cracking and catalytic reforming. In all the cases the goal is to prevent catalysts poisoning. Contaminants mentioned above can cause detrimental effects on catalysts, affect the quality of finished products and produce undesired by-products that can affect the integrity of the plant equipment. Metals poison active sites in most of the supported catalysts used downstream, nitrogen inhibits the acid function HCK catalyst and sulphur poison zeolite based catalyst used in catalytic cracking units [7]. Sulphur content in heavy/medium cuts is typically lower than 5% while nitrogen content is even lower [8].

In Figure 1.2 can be observed a typical flow diagram for a two-stages HCK unit. In refineries, a multistage process is normally preferred over a single-stage reactor since using this configuration the heteroatoms removal (hydrotreating) reactions and the

cracking reactions can take place sequentially but in different reactors. Thus, the adverse effects of ammonia and nitrogen compounds on the HCK catalyst can be avoided by an intermediate gases separation stage.

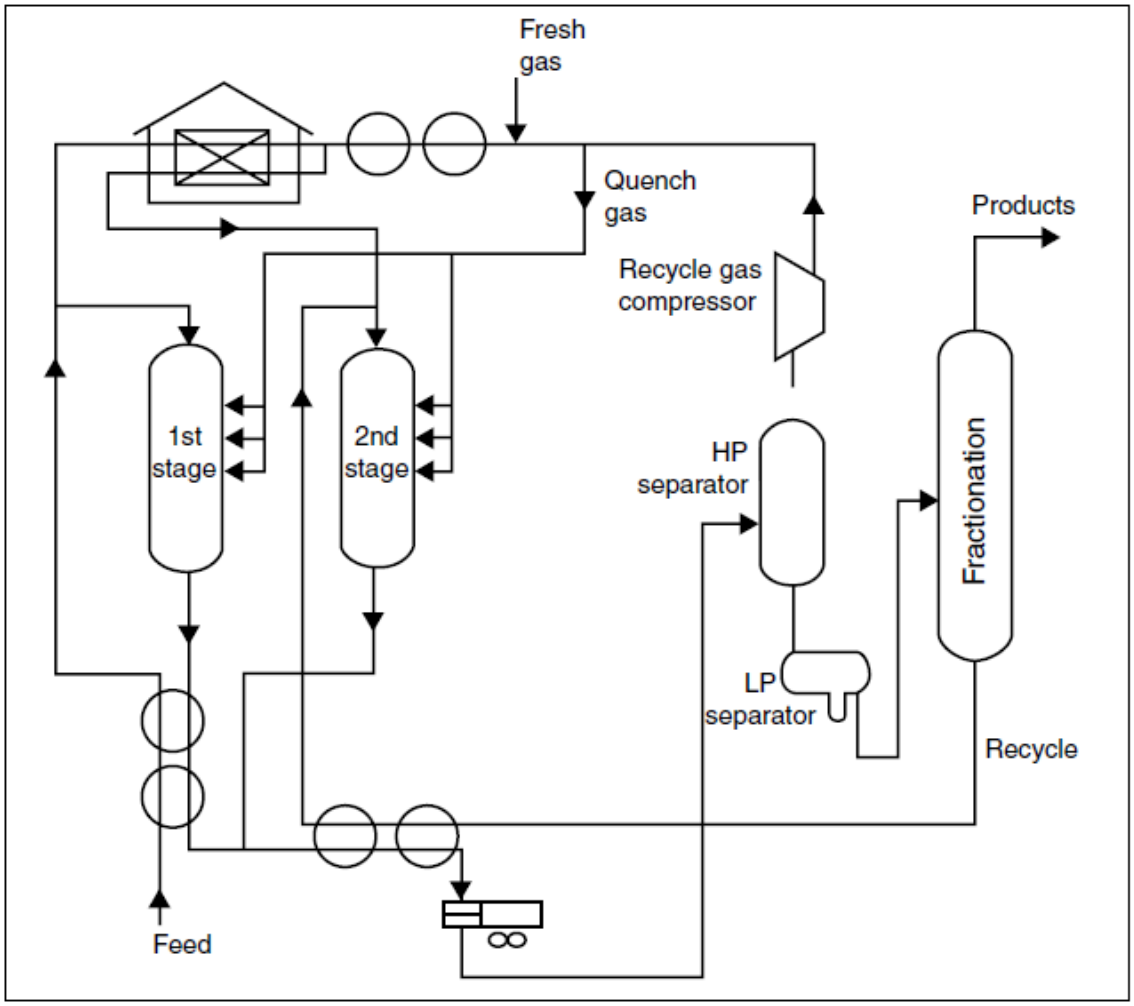

Figure 1.2 A two stage hydrocracking unit [8].

In hydrotreating (HDT) organosulfur and organonitrogen compounds react with hydrogen in the presence of a solid catalyst to produce ammonia and hydrogen sulphide, respectively.

The main types of reaction that takes place in HDT are: Hydrodesulphurization (HDS), Hydrodenitrogenation (HDN), Hydrodemetallization (HDM), Hydrogenation of Aromatics (HAD), hydrodeoxygenation (HDO) and olefin saturation. It must be noted that most crudes contain low levels of oxygen, therefore HDO is of a lesser concern.

The catalysts used for HDT are typically made of nickel-molybdenum (Ni-Mo), cobalt-molybdenum (Co-Mo) or nickel tungsten (Ni-W) supported on alumina (Al_2O_3), often doped by fluorine or phosphorus [9]. In presence of hydrogen, Ni and Co are well known to promote a high level of hydrogenation of unsaturated molecules such as aromatics and olefins. It is well known that the nickel-molybdenum catalysts are more active for hydrogenation than the corresponding cobalt catalysts [10].

In general, any catalyst capable of participating in hydrogenation reactions may be used for hydrodesulfurization and hydrodenitrogenation. The need to develop catalysts that can carry out deep hydrodesulfurization and deep hydrodenitrogenation has become even more pressing in view of recent environmental regulation that limit sulfur and nitrogen emissions. The development of a new generation of catalysts to achieve more efficiently this objective presents an interesting challenge [11]

Due to the high importance of the HDT process in the modern refining schemes, the availability of reliable models is essential to efficiently address plant design, operation monitoring, process optimization as well as catalyst development. The goal of this work is the implementation of kinetic models for HDS and HDN that allow properly describe the removal of these heteroatoms in hydrotreating.

Thus, this work is presented as follows: In Chapter 2, the hydrotreatment process is described with more detail including the reaction mechanisms and a description of the operating variables that mainly influence the composition of the process product.

In Chapter 3, different strategies for HDT modelling as well as techniques for parameters optimization and model validation are exposed. Chapter 4 described details of the models implemented, including all the equations used for kinetic model and reactor model. Finally, the results are shown in Chapter 5 including the differences in the different models implemented and the significance of the kinetic parameters for each case.

2. Hydrotreatment

2.1 General process description

A typical process scheme is illustrated in Figure 2.1. Initially, the feedstock is mixed with hydrogen, preheated in a fired heater up to 300 - 450ºC and later fed to a fixed-bed catalytic reactor under pressures even higher than 100 bar. In the reactor, the sulphur atoms present as heteroatoms in the feedstock are converted to hydrogen sulphide, and the corresponding nitrogen atoms are converted to ammonia [12].

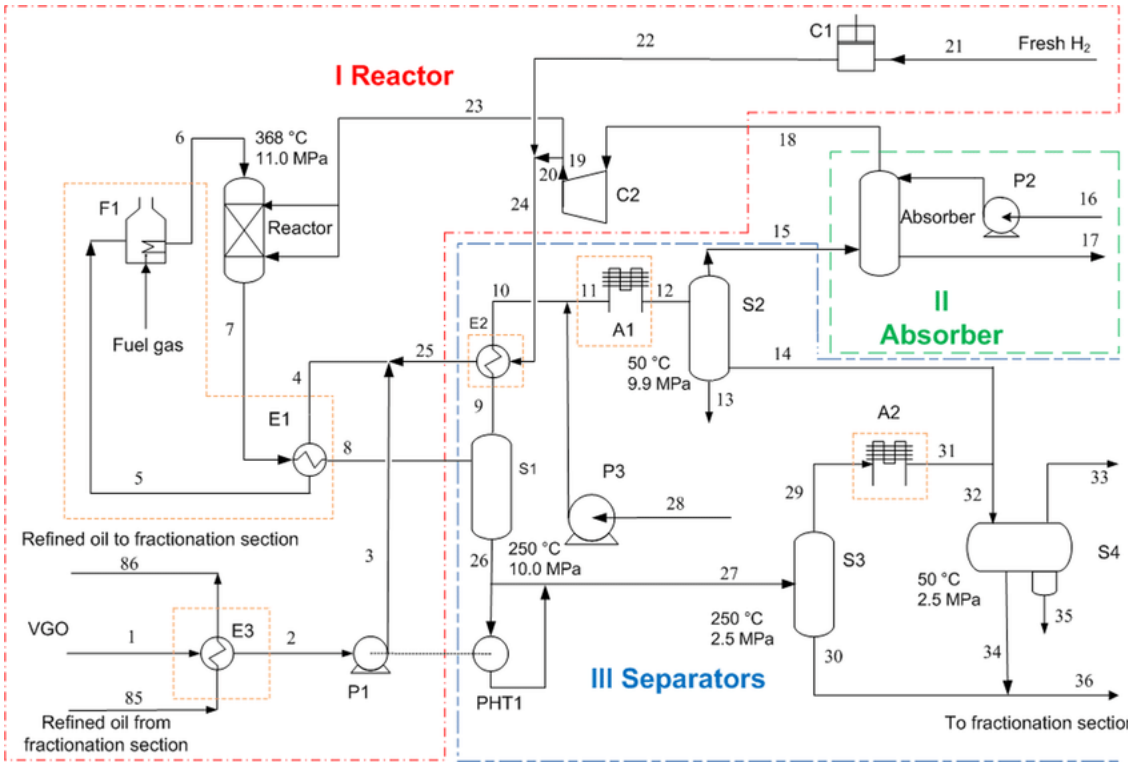

Figure 2.1 VGO hydrotreating process scheme [8].

The reaction products leave the reactor and, after cooled, they enter a liquid/gas separator. The hydrogen-rich gas from the high-pressure separation is recycled and combined with the feedstock, and the low-pressure gas stream rich in light hydrocarbons (C1-C4), H_2S and NH_3 is sent to a gas-treating unit where sour gases are removed. After this process, the gas stream becomes clean and suitable as fuel for the refinery furnaces.

The liquid product stream from hydrotreating is normally sent to a stripping column for removal of dissolved H_2S, NH_3 or other undesirable absorbed components. In cases where steam is used for stripping, the product is sent to a vacuum drier for water removal. Hydrodesulfurized naphtha products are blended or used as catalytic reforming feedstock while hydrotreated Vacuum Gas Oils are further processed in a hydrocracker or a fluid catalytic cracker [7].

2.2 Hydrodenitrogenation

Organonitrogen compounds are undesired in the refining process because, even at low levels, cause an inhibition effect in HCK catalysts. Hydrodenitrogenation consists in removing nitrogen from organonitrogen compounds by breaking the C-N bond to finally release it as ammonia.

In HDN, the direct breakage of C-N bond in heterocyclic aromatic molecules is very unlikely. This reaction is difficult even in exocyclic molecules such as aniline, for which hydrogenation to cyclohexylamine precedes C-N bond breaking. Once the aromaticity is lost and aliphatic C-N bond are formed, C-N bond breaking becomes more likely [13].

Some HDN kinetic models lump all basic-nitrogen compounds and, in another lump, all non-basic nitrogen compounds [14]. It is well-known that non-basic nitrogen compounds are first hydrogenated to basic nitrogen compounds [15] before reactions to eliminate the nitrogen atom from the molecule occur. Thus, a consecutive reaction scheme as shown below can be proposed for the HDN reaction [14]:

$$\text{Nonbasic nitrogen} \rightarrow \text{basic nitrogen} \rightarrow \text{ammonia} + \text{hydrocarbon}$$

Hydrodenitrogenation is more difficult to accomplish than hydrodesulfurization, but the relatively small amounts of nitrogen-containing compounds in conventional crude oil make this of little concern for practical purposes to refiners. The current research focus is oriented towards preparation of better catalysts to remove heavier compounds such as

quinoline or acridine. The trend to high-boiling feedstocks, which are richer in nitrogen, has increased the need to effectively deal with this contaminant [11].

2.2.1 Chemistry of hydrodenitrogenation

In order to understand the mechanisms that lie behind the hydrodenitrogenation reaction, the nitrogen content in the feedstock must be characterized and quantified. The nitrogen content in medium/heavy fractions is typically lower than 4000 wt ppm [16].

In Figure 2.2, basic nitrogen and non-basic nitrogen molecules typically found in VGO are described. Basic nitrogen compounds are the ones where the nitrogen atom only form sigma bonds with the neighbour carbon atoms. In these compounds, the lone pair of electrons on the nitrogen atom is not delocalized in the ring containing the atom and, therefore, it is readily available for reaction with acidic catalyst as a Lewis base [17].

Compounds where the nitrogen atom forms a π-bond are referred as non-basic nitrogen compounds. In non-basic compounds the lone pair of electrons in the nitrogen atom is delocalized over the aromatic ring and, therefore, is unavailable for donation to a Lewis acid.

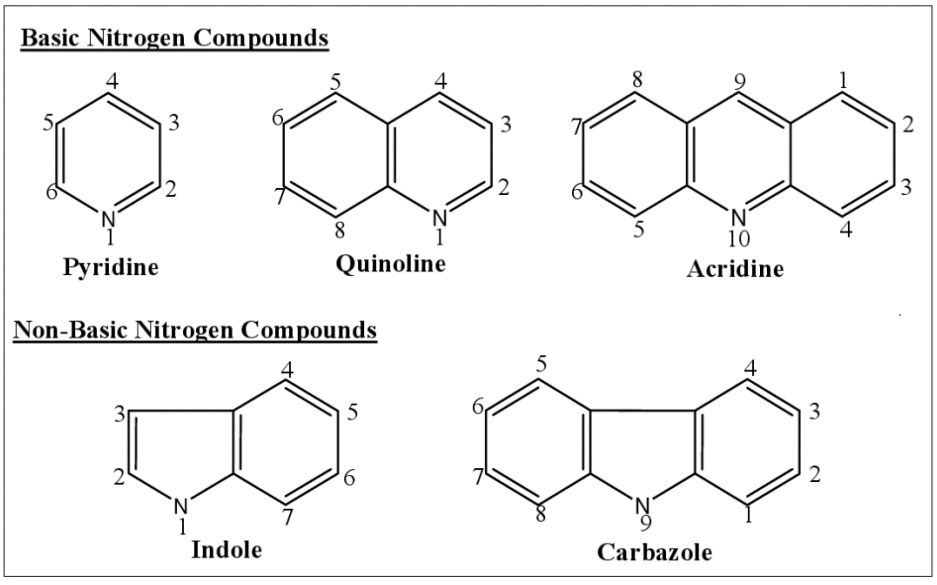

Figure 2.2 Nitrogen-containing compounds of interest in petroleum [18].

One of the most abundant nitrogen-compound presents in fossil fuels is pyridine. In Figure 2.3 it is illustrated the reaction mechanism of pyridine hydrodenitrogenation proposed by Raghuveer [19] using an industrial Ni-Mo/γ-Al_2O_3 catalyst.

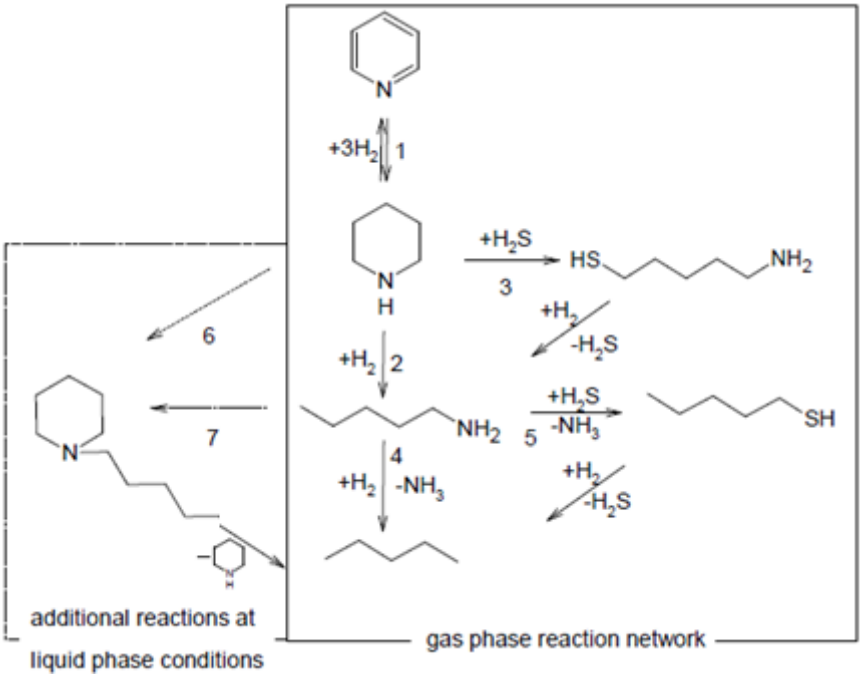

Figure 2.3 Pyridine hydrodenitrogenation network over an industrial catalyst [19].

According to this reaction mechanism, pyridine is first hydrogenated to piperidine. Subsequently, piperidine ring opening yields a primary amine, which further reacts to produce C5 hydrocarbons. In this proposal, both the ring opening and the C-N bond breaking could occur via a H_2S assisted substitution reaction.

The reaction mechanism illustrated in Figure 2.3 can be summarized into 7 main types of elementary reactions to describe the complete conversion of a molecule of pyridine to its product pentane as it follows:

1) Aromatic ring hydrogenation
2) C-N bond scission via β-(H) elimination
3) C-N bond scission via (-SH) substitution
4) Protonation of amines and C-N bond breaking
5) Amine substituted by a (-SH) group

6) Formation of heavier species via pentylamine condensation
7) Formation of heavier species via piperidine condensation

In this work Langmuir Hinshelwood reaction mechanisms accounting for two types of sites, i.e., coordinatively unsaturated sites (*) and sulfur anions (-S_2-), were proposed and corresponding kinetic models were derived to assess the experimentally measured kinetics.

This model successfully captures all phenomena occurring during the reaction at gas phase conditions and provides the basis for an extension towards liquid phase conditions. At both gas and liquid phase conditions, the reaction temperature and H_2S inlet partial pressure were found to be most significantly affecting the selectivity to intermediates and final products.

More complex nitrogen molecules, such as quinoline, are expected to follow a similar reaction pathway. Among basic heterocyclic N-containing compounds, quinoline is a widely used as model molecule in HDN studies. The mechanism for quinoline HDN has been previously studied [20][21] and includes successive hydrogenation of benzenic rings, hydrogenation of aromatic heterocyclic rings and C-N bond cleavage (Figure 2.4).

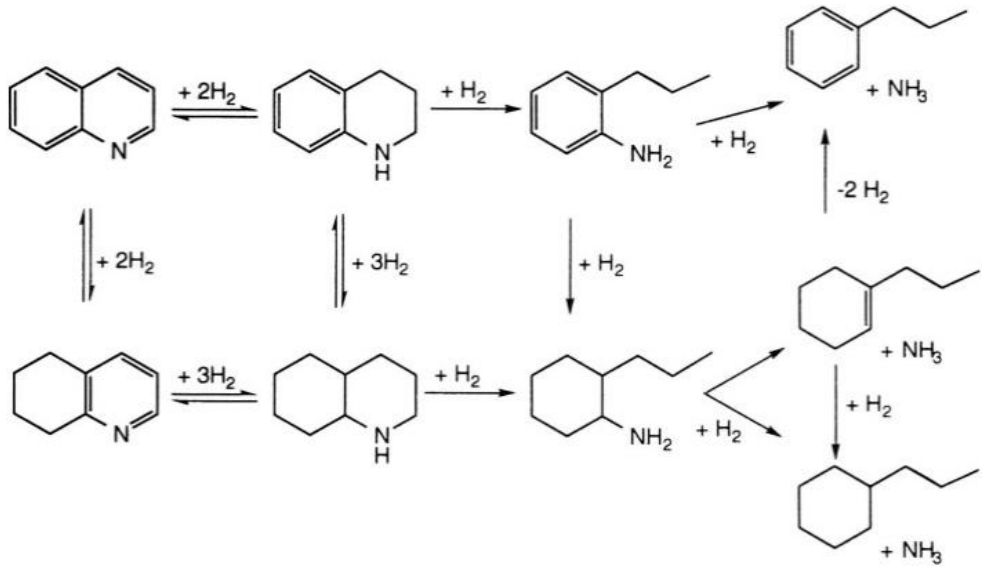

Figure 2.4 Main reaction pathways in quinoline HDN [22].

2.3 Hydrodesulfurization

Hydrodesulfurization (HDS) consists in the hydrotreating operation for sulfur removal. HDS involves exothermic reactions that induce the breaking of C-S bonds, to produce H_2S as a by-product that is separated at a later stage. The sulfur content of crude oils varies from less than 0.05 to more than 10 wt% but generally falls in the range of 1-4 wt% [23]. Crude oil with less than 1 wt% sulfur is referred to as low sulfur or sweet, and that with more than 1 wt% sulfur is referred to as high sulfur or sour.

Because of the large number of sulfur compounds in the different oil fractions, as well as the existing limitations for their identification and measurement, it is very impractical to model all hydrodesulfurization reactions individually. In some kinetic studies about desulfurization, all sulfur compounds are grouped as a single lump and considered as a single global reaction [15][24].

2.3.1 Chemistry of hydrodesulfurization

Techniques for sulfur removal from a petroleum stream depends on the structure of the sulfur compound to be treated. The rates of sulfur removal can vary by several orders of magnitude depending on the molecular structure of the organosulfur compounds. Generally acyclic sulfur compounds such as thiols and disulfides are highly reactive and can be removed under very mild conditions. Saturated cyclic sulfur compounds and aromatic systems in which sulfur is present in six-membered rings are also highly reactive. However, compounds in which the sulfur atom is embedded into a five membered aromatic ring structure, such as thiophens for instance, are much less reactive [25].

There are several different chemical pathways through which sulfur can be removed from a molecule and the preferred pathway changes for different sulfur compound structures. The most common sulfur compounds in fossil fuels are illustrated in Figure 2.5.

Typically, in heavy feedstocks dibenzothiophenes and long chain thiols can be found due to their high boiling points.

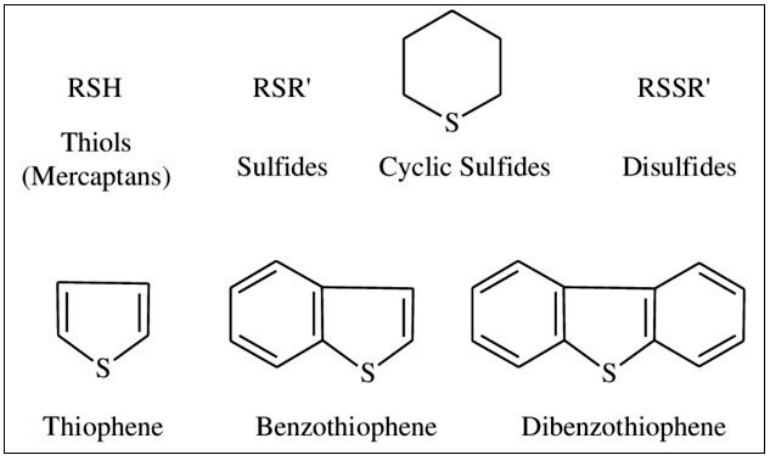

Figure 2.5 Sulfur-containing organic compounds of interest in fossil fuels [26].

In Figure 2.6 the reaction scheme for a thiophene molecule is illustrated showing two major pathways toward desulfurized products. The first one is called direct hydrodesulfurization, in which the sulfur atom is removed from the aromatic structure and replaced by hydrogen, without hydrogenation of any other C-C double bond. The second is called the hydrogenative route, where it is assumed that at least one aromatic ring adjacent to the sulfur containing ring is hydrogenated before the sulfur atom is removed and replaced by hydrogen [25].

In the first pathway an aromatic ring may be hydrogenated after sulfur removal. This often leads to confusion in interpreting the results of experimental data as both routes can produce the cyclohexylbenzene as final product. It should be noted that the hydrogenation pathways are subject to thermodynamic equilibrium constraints [27].

The hydrogenative pathway involves the initial hydrogenation of one or more of the carbon-carbon double bonds adjacent to the sulfur atom in the aromatic system. Hydrogenation destabilizes the aromatic ring system weakening the sulfur-carbon bond and providing a less sterically hindered environment for the sulfur atom. This way the interaction of the sulfur atom with the metal insertion on the catalyst surface is facilitated. Figure 2.6 illustrates both reaction schemes including details of the active sites [28].

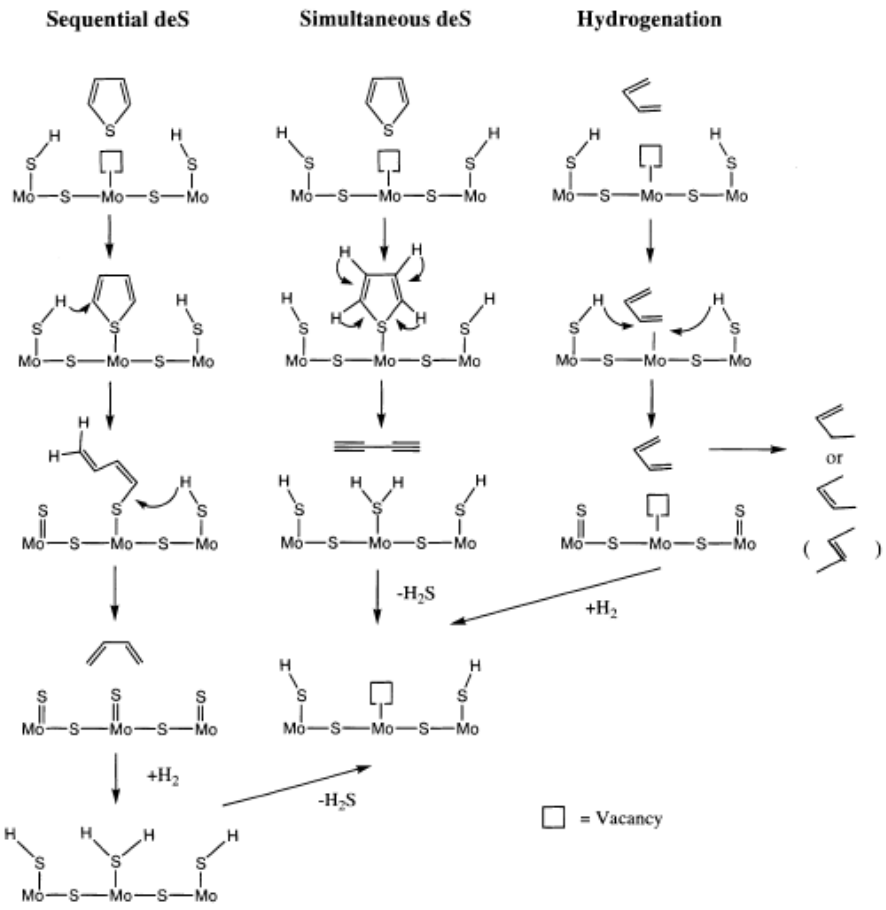

Figure 2.6 Vacancy Model of the HDS mechanism [25].

Due to its boiling range between 150ºC and 550ºC, in medium/heavy fractions is expected to find aromatic sulfur molecules with higher molecular weight than thiophen. In Figure 2.7 it is represented a scheme that shows different reaction pathways for the HDS of 4,6-Dimethyldibenzothiophene (4,6-DM-DBT), a typical complex high-molecular-weight molecule that can be found in vacuum gas oils.

In this scheme the reaction rates were calculated for a simple model assuming pseudo first-order rate constants in the presence of a heterogeneous catalyst (Ni-Mo) [13]. According to the described reaction rates, the hydrogenation route is faster than the direct C-S bond breaking.

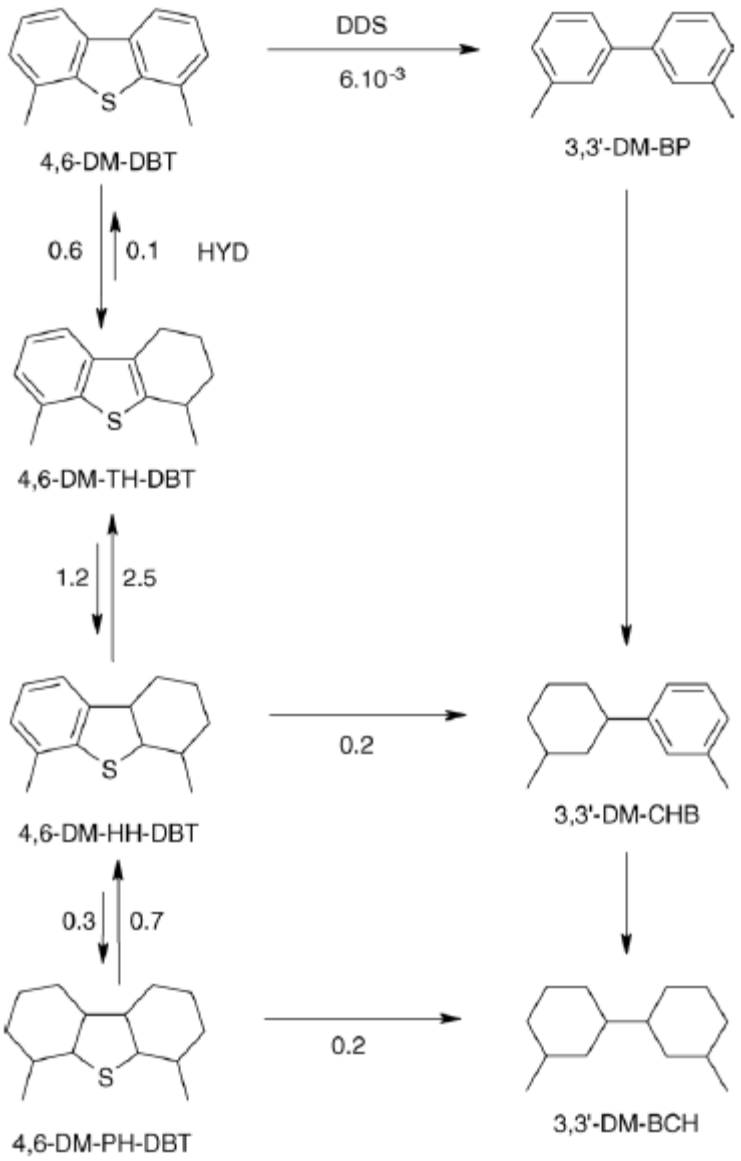

Figure 2.7 Reaction network of the HDS of 4,6-DM-DBT [13].

In comparison with other components, 4,6-DM-DBT has proved to be a molecule with low reactivity. A possible solution would be to find the means of suppressing the steric hindrance brought by the alkyl groups in 4,6-DM-DBT in order to increase its reactivity [29].

Detailed kinetic equations for the conversion of thiophene, benzothiophene and dibenzothiophene has been extensively investigated in the past [30][31][32]. The existence of two different active sites, σ-sites for the hydrogenolysis reactions and τ-sites for the hydrogenation reactions, was one of the main conclusions in those researches. In

addition, they accounted for competitive adsorption of H_2 and H_2S and other reacting species on both sites.

2.4 Hydrotreating reactor

Hydrotreating units for light feeds are carried out in two-phase (gas and solid) fixed-bed reactors. However, when the boiling point of the feed increases, three phases will be found: hydrogen (H_2), a liquid-vapor mixture of the partially vaporized feed, and the solid catalyst. This reaction system is called trickle-bed reactor (TBR), which is referenced in the literature as a reactor in which a liquid phase and a gas phase flow concurrently downward through a fixed-bed of catalyst particles while reactions occur [33].

The kinetic modelling of a TBR is based on the two-film theory [34]. This theory can be applied to hydrotreating as it is illustrated in Figure 2.8.

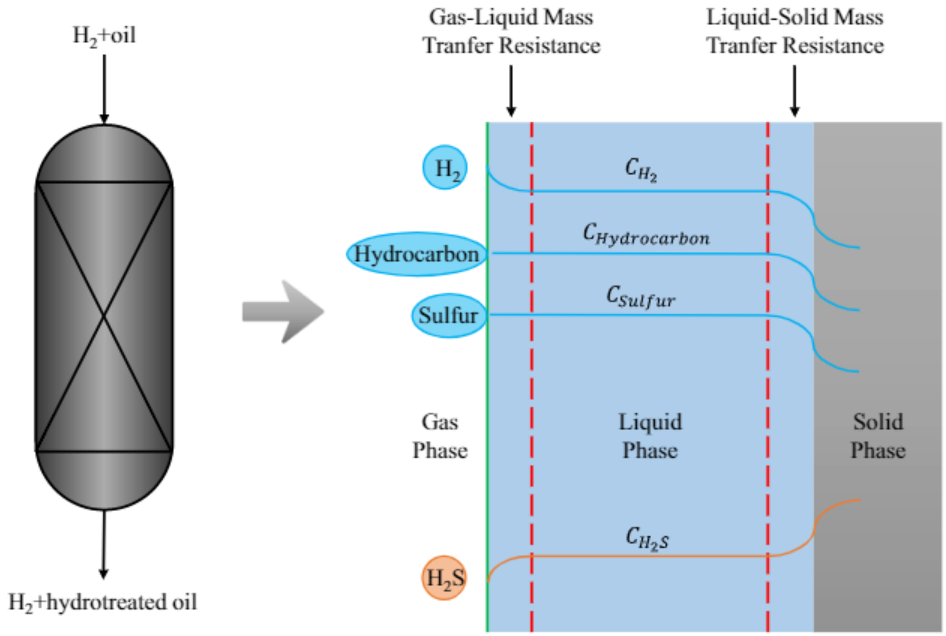

Figure 2.8 Concentration profiles in a trickle-bed reactor [34].

In a trickle bed reactor, the gas and liquid reactants are effectively contacted over the surface of a solid catalyst in a co-current down-flow mode. In the trickle flow regime, the liquid reactant flowing down through the reactor forms a thin film around the solid catalyst. The gas reactant being the continuous phase fills the remaining void space of the

catalyst bed and flows separately. The trickling flow regime appears at relatively low gas and liquid flow rates and is classified as low-interaction regime of three-phase reactor systems [35].

2.5 Operating conditions

The main hydrotreating operating variables are bed temperature, H_2 partial pressure, H_2/oil ratio and LHSV (Liquid Hourly Space Velocity). The values of these operating variables depend on the quality of the feedstock and the desired product specifications. For instance, high-boiling petroleum feedstock such as VGO need more severe conditions than a low-final boiling point fraction such as naphthas [36].

2.5.1 Temperature

Generally, increasing temperature leads to higher HDS and HDN conversions. However, increasing the reaction temperature implies higher costs due to a higher energy consumption. In addition, a higher operation temperature results in an accelerated catalyst deactivation and, therefore, a short catalyst operating life [37]. Moreover, thermal cracking effects can occur when working at elevated temperatures [38].

In general, hydrotreating operating temperature should be kept as low as possible while maintaining the desired product quality [39].

2.5.2 H_2 partial pressure

In gas-liquid-solid reactors such as trickle bed reactor, the gaseous reactant (in HDT case, the hydrogen) dissolves into the liquid prior to its diffusion into the solid, the catalyst. The overall reaction rate with respect to the gaseous reactant is a direct function of the efficiency of the gaseous reactant to dissolve into the catalyst through the liquid phase [40].

Henry's Law states that a gas dissolution is proportional to its partial pressure above the liquid. Thus, an increase in H_2 partial pressure will increase the concentration of H_2 in the liquid phase and, therefore, it will enhance hydrotreating conversion. A reduction in H_2 partial pressure below adequate level results in catalyst deactivation due to coke formation. Design value for H_2 partial pressure is an economic optimum which balances the catalyst life against operating costs [36].

Excessively high H_2 partial pressure may merely saturate the surface of the catalyst, which is a plus from a catalyst deactivation standpoint without significantly improving hydrotreating activity [41].

H_2 partial pressure is also related to the purity of the hydrogen stream that enters the reactor. As shown in Fig. 1-02 and Fig. 2-01, un-reacted H_2 is usually recovered from the reactor effluent and then mixed with fresh H_2 to increase the purity before being recycled into the reactor. Due to the high cost of H_2, if it is not recovered from the reactor gaseous effluent and recycled, the hydrotreating operation is compromised in terms of its economic viability [41].

2.5.3 H_2/oil ratio

H_2/oil ratio is the ratio of total gas fed into the reactor to the amount of feedstock. This variable is of great importance and if kept too low it will result in rapid catalyst deactivation. In general, the minimum H_2/oil ratio should be at least 4 times the amount of hydrogen consumption [36]. Bej et al. [14] reported that for HDS and HDN there is an optimal value for H_2/oil ratio which depends on the nature of the feedstock and the values of the other operating variables.

2.5.4 LHSV

The Liquid Hourly Space Velocity (LHSV) is defined as the ratio of the volumetric flow rate (hourly) of the liquid feedstock to the volume of the catalyst bed. LHSV is the inverse of the residence time. A decrease in the LHSV usually leads to an improvement of the hydrotreating conversion. Nevertheless, an extreme reduction of LHSV may cause malfunctions in the operation due to hydraulic considerations [42].

Severe reduction of LHSV triggers channelling which results in poor liquid distribution and underutilization of the catalyst. On the other hand, operating at too high LHSV values does not only reduce the contact time between the catalyst and the feedstock but also it increase the reactor pressure drop and may present some hydraulic problems [36].

3. Modelling

3.1 Hydrotreatment modelling approaches

There are many challenges involved in hydrotreatment modelling. One of them is the molecular diversity of hydrocarbons, organosulfur, organonitrogen and other molecules with heteroatoms existing in the feedstock. This fact derives in an important number of reactions with their respective mechanisms that need to be considered if a fundamental representation of the process is intended. A more general description of the phenomena could also be helpful to study the underlying kinetics. Thus, according to the level of detail given to the reaction mechanisms, the hydrotreatment modelling could be tackled according to two different approaches: discrete lumping methods and fundamental kinetics.

3.1.1 Discrete lumping method

The lumping approach consists of regrouping chemical compounds by similar properties in clusters called lumps. The lumps are then considered as homogeneous ensembles that mimic a molecule, which allows to pose kinetic formulations as normally made for real compounds. This approach is often used for processes where the exact molecular characterization of the reactant mixture is difficult or impossible because of the complexity of the feedstock, as is the case in the majority of petroleum processes (catalytic reforming, hydrotreating, catalytic cracking, thermal cocking etc.) [43].

The development of a lumping approach usually proceeds through the following steps:

1) Description of the feedstock by choosing a set of lumps.
2) Description of the relationships between the lumps by building a kinetic network of lumped reactions.
3) Proposal of the rate equations and their associated parameters.

4) Determination via optimization of the model parameters that allows a better description experimental data.

The choice of lumps depends on the level of detail that could be obtained using the available analytical techniques and, on the purpose of the model. For a comprehensive validation, the more detail in the kinetics, more detailed must be the characterization of feed and products.

Lumped kinetic models are relatively easy to develop because the number of lumps and the number of reactions remain could be kept limited to a tractable number. Moreover, due to the multicomponent characteristics of the lumps, the reaction pathways are generally global with no intermediate species and the kinetic rate equations are often simple (pseudo-order reactions, Langmuir-Hinshelwood approach in heterogeneous kinetics, etc) which is a simplification of the actual underlying mechanisms. Their kinetic parameters (pre-exponential factors, activation energies, adsorption constants, etc) are often determined by minimizing the deviations between model and experimental data coming from pilot units or industrial plants [43].

For lumped models to be robust and feed independent, a wide variety of experimental data in terms of operating conditions and feedstock composition is needed.

One of the first lumped models developed in hydrotreating was at IFPEN for the Atmospheric Gas Oil (AGO) hydrotreating, which consisted in a 6-lump model accounting for only 1 sulfur lump for dibenzothiophenes, 1 nitrogen lump for carbazoles and 4 hydrocarbon lumps representing saturates, monoaromatics, diaromatics and triaromatics [44]. The rate equations were derived from the following hypotheses: the existence of two types of active sites for hydrogenation and for hydrogenolysis, Langmuir-Hinshelwood approach and equilibrium for adsorption/desorption reactions.

López Garcia [45] improved the accuracy of the hydrodesulfurization prediction by introducing 3 sulfur lumps which represent the 3 most refractory sulfur classes of found in AGO: DBT, 4-M-DBT and 4,6-DM-DBT. This extended reaction network contained

9 overall reactions and the experimental domain was extended in terms of operating temperature and LHSV.

Further improvements involved the introduction of thermodynamic constraints for the reversible reactions and the use of a two-phase plug flow reactor. The largest extensions concerned the feedstocks, where 24 different types of industrial gas oils were included: straight run gas oils, LCO, coker gas oils, etc. This feed diversity is particularly important to confer a high degree of generalization capacity to the model [43].

3.1.2 Single-events methodology

The single-events microkinetic (SEMK) methodology was first developed in the 1980s by Baltanas et al. [46] as a method of capturing the fundamental chemistry of HCK of linear alkanes. The methodology has been later extensively applied to complex reaction mixtures [47]

Classical modelling is usually performed using concepts and reaction schemes such as proposed by Langmuir and Hinshelwood or Eley and Rideal. In this type of modelling, various possible mechanisms are proposed and the corresponding rate equations are derived considering different elementary steps as rate determining [48].

As opposed to classical modelling, the SEMK methodology allows simulating complex mixture conversion considering all the elementary reactions occurring in the bulk or on the catalyst surface based on a limited number of adjustable parameters. Single-Event is calculated on the molecular level so detailed information about feed and products composition is required. A comprehensive molecular analysis of complex mixtures comes within reach using 2D GC. However, present-day analytical techniques cannot supply such detailed compositions on a routine basis, as is the case for bulk properties determination.

A systematic determination of a detailed composition of complex mixtures departing from bulk properties can be achieved by so-called feed reconstruction [49].

The molecules within a single species are considered to be in equilibrium. The single events concept is based on the number of possible ways in which one species can be transformed into another compared to the total number of possible transformations via the same activated complex. Departing from the Transition State Theory (TST) [43] the rate coefficient for an elementary step can be written as:

$$k = \frac{\sigma_{gl,r}}{\sigma_{gl,r\neq}} \frac{k_B T}{h} \exp\left(\frac{\Delta S^{0,\neq}}{R}\right) \exp\left(\frac{\Delta H^{0,\neq}}{RT}\right) \qquad \text{Equation 3.1}$$

Where:

k	kinetic coefficient (s^{-1})
$\Delta S^{0,\neq}$	Reaction entropy (J mol^{-1} K^{-1})
$\Delta H^{0,\neq}$	Reaction enthalpy (J mol^{-1})
R	Gas constant (8.314 J mol^{-1} K^{-1})
T	Reaction temperature (K)
H	Planck constant ($6.626 \cdot 10^{-34}$ m^2 kg s^{-1})
kB	Bolzmann constant ($1.381 \cdot 10^{-23}$ m^2 kg K^{-1})
$\sigma_{gl,r}$	Global symmetry number of reactant.
$\sigma_{gl,r\neq}$	Global symmetry number of transition state.

The energy terms in Equation 3.1 can be calculated using the Benson group contribution method [50] while the number of single events (n_e), defined in Equation 3.2 depends only on the symmetry of the intermediate and the product and essentially quantifies the number of structurally indistinguishable ways in which an elementary step can occur and is correspondingly:

$$n_e = \frac{\sigma_{gl,r}}{\sigma_{gl,r\neq}} \qquad \text{Equation 3.2}$$

The description of the hydrodenitrogenation kinetics according to single-event methodology was investigated in Raghuveer's work [19]. In this work a two-site model was proposed for the construction of the comprehensive SEMK pyridine hydrodenitrogenation over a sulphided NiMo/γ-Al_2O_3 catalyst. This work considered

chemisorption equilibria of the organonitrogen compound over the catalyst surface followed by a reaction network consisting in 9 reaction types.

In complex mixtures, such as VGO, AGO, CGO, etc., the reaction network of the elementary steps is large and complex. However, this complexity can be tackled by applying single-event concept, which drastically reduces the number of kinetic coefficients that describe the global reaction system [51].

3.2 Kinetic parameter estimation

Model parameters whose value are not available beforehand can be estimated via regression using experimental data. Pre-exponential factors, activation energies, orders of reaction and adsorption constants can be listed as usual parameters. Once all parameters are tuned to minimize the error with given experimental data, the model can be used as a prediction tool for model-based decision for process design, to determine optimum operation conditions or to perform model based process control [52].

Depending on the developed model, a linear or non-linear regression approach could be applied to estimate kinetic parameters from experimentally determined reaction rates. [53].

3.2.1 Optimization methods

Given the complexity of the mechanisms involved in hydrotreating models, which are typically highly non-linear, a non-linear regression must be used for parameter estimation, and the task turns into a non-linear optimization problem. [54]. There is a big collection of methods that can be used for solving: Gauss-Newton, Levenberg-Marquardt, gradient methods, such as steepest descent; direct search methods, such as Nelder-Mead simplex, etc [55]. The chose optimization method depends on the range of the available information about the mathematical model: initial estimates, boundaries, constraints,

analytical derivative expressions, etc. The more information about the model, the more reliable optimum will be.

3.2.2 Initialization of parameters

Finding the optimal solution using any nonlinear parameter estimation method strongly depends on the initial guess of parameters values. The initialization of parameters is a usual challenge in nonlinear parameter optimization where the method may often converge to local minima and, in the worst scenario, does not find any solution [56].

If the kinetic model and the corresponding parameters have been reported previously by other authors, no matter the differences in reaction conditions, catalyst, feed, reaction system, at least the order of magnitude reported can be used as initial guess [57].

When there are not reported values available, an iterative analysis of orders of magnitude of the parameters should be initially performed. This analysis can be tedious since it implies several calculations of the objective function for different sets of parameters, starting with initial guesses and then iterating and modifying the parameters one by one. For any modification of a parameter, the change in the objective function is examined and hence, the influence of each parameter can be determined.

On the other hand, an initial guess of parameter values can also be obtained using Monte Carlo method [58], which consists in the following three steps: initial guess of parameters is determined using random numbers, (2) with this initial guess of parameters the objective function is calculated and (3) this procedure is repeated N times ($N > 1000$) and the minimum of the N values of the objective function is determined. The set of initial guesses that corresponds to this minimum can be used as initial parameters in our nonlinear optimization problem.

4. Methodology

The applied methodology consisted in four stages: Data set Analysis, Model Formulation, Parameters Determination and Model Evaluation. In Figure 4.1 a scheme that represents the methodology process followed in this work is illustrated. Once the model is evaluated the method considers adjustments over the original formulation.

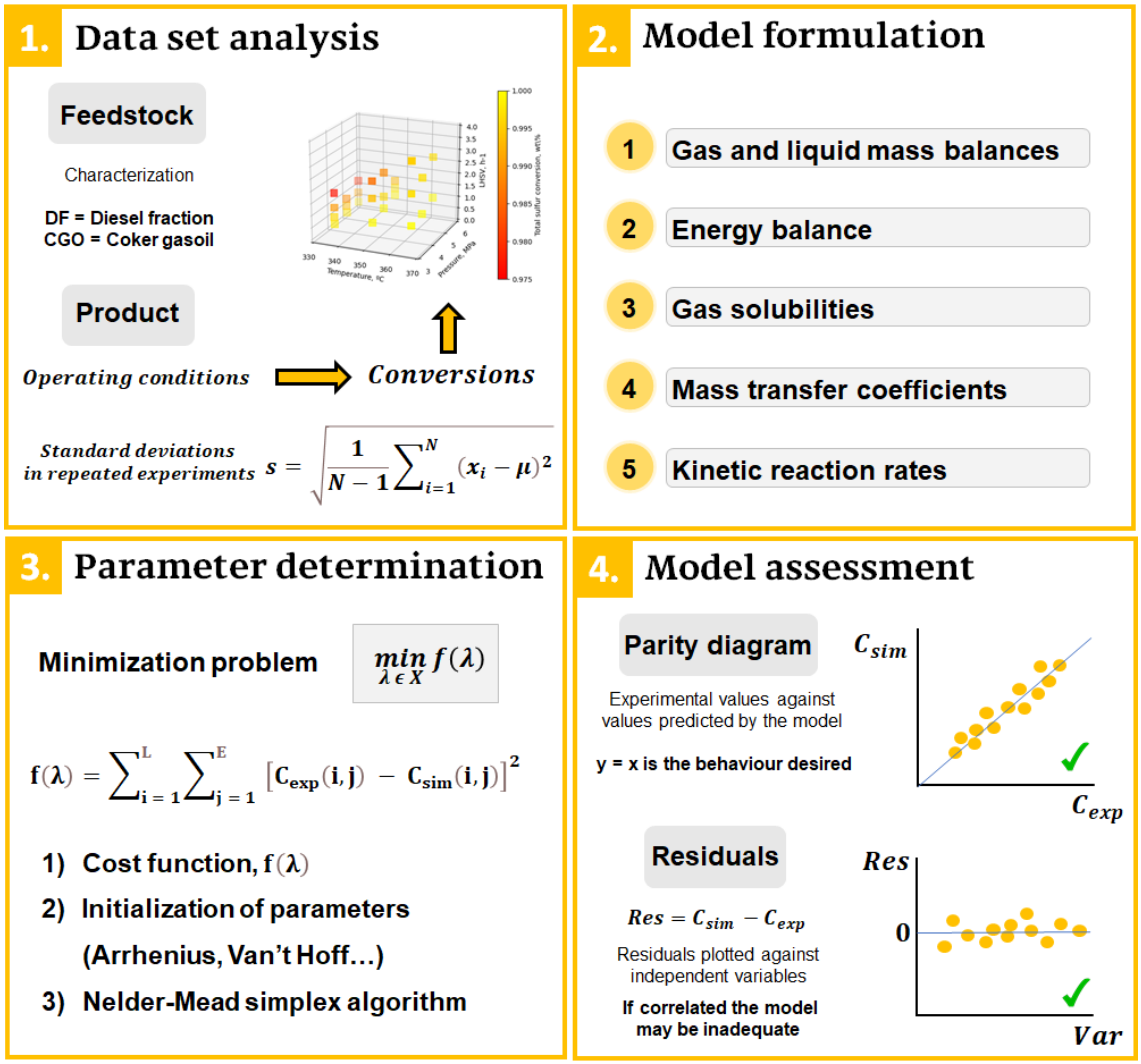

Figure 4.1 Methodology scheme

4.1 Data set analysis

Table 4.1 collects the experimental data of the feedstocks used in a pilot-plant rig. There are four different feedstocks, which correspond to the mixture of two petrol fractions: Diesel fraction (DF) and Coker Gasoil (CGO). This table collects the total contents of

sulfur and nitrogen as well as the sulfur content of the different lumps that are used in the kinetic models.

Table 4.1 Feed sulfur and nitrogen content.

Feed	Total S, ppm	Total N, ppm	Mercaptans, ppm	Thiophenes, ppm	DBT, ppm	Alkyl DBT, ppm
DF	20620	186	10289	9107	948	277
CGO	22860	766	19776	2822	206	56
DF+15% CGO	20956	254	11712	8164	837	244
DF+30% CGO	21292	360	13135	7222	725	210

A summary of the 53 experiments that were run to study the hydrotreating reactions is given in Table 5.3. All the experiments were carried out at different conditions (pressure, reaction temperature and liquid hourly space velocity) and the composition in the product was analysed afterwards leading to these results.

Table 4.2 Summary of experimental results.

Nº	Feed	T, ºC	P, MPa	LHSV, h -1	Total S, ppm	Total N, ppm	Mercaptans ppm	Thiophenes, ppm	DBT, ppm	Alkyl DBT, ppm
1	DF	340	3.5	2	382.4	78.3	64.2	178.9	80.5	58.8
2	DF	335	3.5	1.8	492	82	96.4	218.6	103.4	73.3
3	DF	335	3.5	1.2	204	44	15.1	111.1	42	35.7
4	DF	335	3.5	0.8	59.3	17.6	1.03	23.6	18.2	16.5
5	DF	365	3.5	0.9	9.6	4	0	0	0.9	0.4
6	DF	365	3.5	2	45	27.8	1.6	15.5	14.2	13.9
7	DF	365	3.5	3.5	234	75	50.6	99.2	43.6	40.5
8	DF+30%CGO	335	3.5	1.8	535	139	114	243	113.7	64.2
9	DF+30%CGO	335	3.5	1.2	268	87	45	119	60.6	43.8
10	DF+30%CGO	335	3.5	0.8	132	40	2	70	29.8	30.3
11	DF+30%CGO	350	3.5	0.8	29.5	23.2	0	1.3	7.3	7.5
12	DF+30%CGO	350	3.5	1.8	155	95	9.8	67.7	37.2	40.7
13	DF+30%CGO	350	3.5	2.5	245	134	33	107	56.2	52.6
14	DF	340	3.5	2	385	84	58	173	86	68
15	DF+30%CGO	365	3.5	3.5	204	136	31	69	49	56
16	DF+30%CGO	365	3.5	0.9	11.7	13.3	0	0.9	1	0.9
17	DF+15%CGO	350	4.3	1.5	71.9	24.8	0.8	17.7	24.9	28.6
18	DF+15%CGO	350	4.3	1	28.7	8.4	0	1.11	6.7	6.1
19	DF+15%CGO	350	4.3	2.5	245	70	31	116	51	47
20	DF+15%CGO	335	4.3	1.2	241	41	15.9	127	52	46
21	DF+15%CGO	335	4.3	0.9	134	21.9	17	64	28	25
22	DF+15%CGO	335	4.3	0.6	52	7.3	3.2	20.6	16.2	10.7
23	DF+15%CGO	365	4.3	2.5	62	41	1	17.1	20.3	23.7

24	DF+15%CGO	365	4.3	1	8.6	4.5	0.8	0	0.6	0
25	DF	340	3.5	2	399.5	75.3	64.1	194.7	83.3	57.3
26	DF	350	3.5	0.8	10.3	3.7	1.1	0	2.4	0.8
27	DF	350	3.5	1.8	97	30.9	2.3	47	25	22.4
28	DF	350	3.5	2.5	235	66	24	104	58	50
29	DF+15%CGO	350	3.5	0.8	18	7	0.3	1.1	4.2	2.8
30	DF+15%CGO	350	3.5	1.8	128	54	3.6	56	35	34
31	DF+15%CGO	350	3.5	2.5	263	91	28	112	76	75
32	DF+15%CGO	335	3.5	1.8	483	98	92	228	102	61
33	DF+15%CGO	335	3.5	1.2	256.7	58.5	28.7	130	54.5	43.5
34	DF+15%CGO	335	3.5	0.8	76	20.6	1.6	32.3	22.8	19.4
35	DF+15%CGO	365	3.5	0.9	7.9	4.9	1.4	0	0.6	0
36	DF+15%CGO	365	3.5	2.2	63.6	53.6	1.2	22.4	18	22
37	DF+15%CGO	365	3.5	3.5	98	79	1.9	34	26.8	35
38	DF+15%CGO	335	3.5	0.5	33	10.3	1.5	13.4	10.7	7.4
39	DF+15%CGO	350	5.1	1.8	143	23.6	9.7	74	32	26
40	DF+15%CGO	350	5.1	1.2	34.6	5.5	0	8.3	11.5	7.8
41	DF+15%CGO	350	5.1	1.5	58.7	7.9	0.4	19.7	16.9	14.4
42	DF+15%CGO	335	5.1	1.1	191	13.3	21	104	37	28
43	DF+15%CGO	335	5.1	0.7	51	4.1	1.2	25.3	15	8.8
44	DF+15%CGO	335	5.1	1.6	432	44	82	218	80	52
45	DF+15%CGO	365	5.1	1.3	7.5	3.7	0.3	1.5	1.9	1.1
46	DF+15%CGO	365	5.1	3	65	21.2	3.7	24.8	18.6	18
47	DF+15%CGO	350	5.1	1.5	63	9.3	1.8	29	18.1	13.9

4.2 Model formulation

4.2.1 Reactor model

In this part of the methodology, the equations of the reactor model are described.

4.2.1.1 Model assumptions

The model was developed according to the following assumptions:

1. Constant gas and liquid velocities across the reactor section.
2. No radial concentration gradients.
3. The mass transfer effects can be described by linear mathematical equations.
4. Constant catalyst activity in time.
5. No vaporization or condensation of sulfur and nitrogen compounds.
6. Steady state regime for the reactor (no accumulation terms).
7. All reactions take place in liquid phase.

8. All the reaction rate constants are described by the Arrhenius law.

4.2.1.2 Gas phase mass balance

The independent variable to integrate the reactor is z, the reactor length. It is considered that no reactions take place in the gas phase and the mass-balance equations for the gas compounds (H_2, H_2S and NH_3) can be described as:

$$\frac{u_G}{RT}\frac{dP_i^G}{dz} + k_i^G a_L \left(\frac{P_i^G}{H_i} - C_i^L\right) = 0 \qquad \text{Equation 4.1}$$

Where u_G represents the superficial velocity of the gas, R is the universal gas constant, T represents the reaction temperature, P_i^G are the partial pressures of the gas, $k_i^G a_L$ represents the mass transfer coefficient between the gas and the liquid phase, the liquid-phase concentrations of the gas compounds in equilibrium with the bulk are represented by the Henry's law, with the Henry's coefficient H_i for each component and C_i^L is the concentration of the component in the global liquid phase.

4.2.1.3 Liquid phase mass balance

In Equation 4.2, the mass balance for hydrocarbons is represented assuming that all of them are only present in the liquid phase. Since goal is focused on HDS and HDN reactions, only nitrogen and sulfur hydrocarbon compounds are the considered reactive species.

$$u_L \frac{dC_i^L}{dz} + k_i^S a_S \left(C_i^L - C_i^S\right) = 0 \qquad \text{Equation 4.2}$$

In Equation 4.2, u_L represents the superficial velocity of the liquid, C_i^S is the concentration of the component 'i' in the liquid phase at the catalyst surface and $k_i^S a_S$ is the liquid-solid mass transfer coefficient. Based on the model, the driving force in the liquid-solid interface can be described as:

$$k_i^S a_S \left(C_i^L - C_i^S\right) = -v_i\, r = -v_i\, \rho_B\, r_j \qquad \text{Equation 4.3}$$

Where ρ_B is the bulk density, v_i represents the stoichiometric coefficient for component i, r_j is the reaction or set of reactions in which the component i intervenes.

As a result of both Equation 4.2 and Equation 4.3, the plug-flow model equation is obtained:

$$\frac{dC_i^L}{dz} = \frac{\rho_B \, r_j}{u_L} \qquad \text{Equation 4.4}$$

The molar concentration of the components in the liquid phase at the reactor inlet can be calculated using the molecular weights and the density of the oil fraction together with the mass fraction:

$$C_i^L = \frac{\rho_L}{M_i} \cdot w_i \qquad \text{Equation 4.5}$$

The density ρ of the oil at process conditions can be determined by the Standing-Katz correlation [59]:

$$\rho(P,T) = \rho_0 + \Delta\rho_P - \Delta\rho_T \qquad \text{Equation 4.6}$$

Where ρ_0 represents the density at standard conditions (15.6ºC and 1 atm), that can be obtained with the specific gravity value:

$$SG = \frac{141.5}{API+131.5} \qquad \text{Equation 4.7}$$

The API gravity is a typical measure of density for oil fractions.

The pressure dependence of density can be calculated by the following expression:

$$\Delta\rho_P = [0.167 + 16.181 \cdot 10^{-0.0425 \cdot \rho_0}] \cdot \left(\frac{P}{1000}\right) - 0.01 \cdot [0.299 + 263 \cdot 10^{-0.0603 \cdot \rho_0}] \cdot \left(\frac{P}{1000}\right)^2 \qquad \text{Equation 4.8}$$

Where P is the pressure in psia. Since the density drops with rising temperature, a temperature correction (in ºR) is given by the following equation:

$$\Delta\rho_T = \left[0.0133 + 154.2 \cdot (\rho_0 + \Delta\rho_{P)}{}^{-2.45}\right] \cdot (T - 520) - \left[8.1 \cdot 10^{-6} - 0.0622 \cdot 10^{-0.764 \cdot (\cdot \rho_0 + \Delta\rho_p)}\right] \cdot (T - 520)^2 \qquad \text{Equation 4.9}$$

4.2.1.4 Gas solubilities

The mass balance equations assume that the gas-liquid equilibrium for this mixture can be described by the Henry's law. The Henry coefficient H_i can be obtained from solubility coefficients λ_i:

$$H_i = \frac{v_N}{\lambda_i \cdot \rho_L}$$ Equation 4.10

Where v_N is the molar gas volume at standard conditions and ρ_L represents the density of the liquid phase under process conditions. Taking data from the literature [24] it is possible to obtain the solubility for the gas components using the following correlation:

$$\lambda_{H_2} = -0.559729 - 0.42947\,T + 3.07539 \cdot 10^{-3}\,\frac{T}{\rho_{20}} + 1.94593 \cdot 10^{-6}\,T^2 + 0.835783 \cdot \frac{1}{\rho_{20}^2}$$ Equation 4.11

Where T is the temperature, ρ_{20} represents the density at 20ºC, and the hydrogen solubility is given in (Nl H_2)/[(kg oil) · (MPa)].

The solubility of hydrogen sulfide in mineral oil fractions can be also calculated using a different correlation [24] represented in Equation 4.12. This solubility is given in (Nl H_2S)/[(kg oil) · (MPa)].

$$\lambda_{H_2S} = exp\,(3.3670 - 0.008470\,T)$$ Equation 4.12

Chacón et al. [60] derived in the following correlation as a function of temperature in [K] for solubility coefficient calculation in (Nl NH_3)/[(g oil) · (MPa)]

$$\lambda_{NH_3} = \frac{1}{8.552 \cdot 10^{-2} + 2.233 \cdot 10^{-6} \cdot T^{2.79}}$$

4.2.1.5 Gas-liquid Mass Transfer coefficient

The gas-liquid mass transfer coefficient is a function of the liquid superficial velocity, G_L. For its determination, it is possible to use a correlation from the literature [61]:

$$\frac{k_i^L \cdot a_L}{D_i^L} = \alpha_1 \cdot \left(\frac{G_L}{\mu_L}\right)^{\alpha_2} \cdot \left(\frac{\mu_L}{\rho_L \cdot D_i^L}\right)^{1/2}$$ Equation 4.13

Where the term $k_i^L \cdot a_L$ represents the mass transfer coefficient, ρ_L is the density of the liquid that can be determined with Equations 4.6 – 4.9. The coefficients α_1 and α_2 are related to the mass transfer surface and the geometry of the particles and are specific for each bed. The dynamic liquid viscosity, μ_L, can be calculated as a function of temperature and oil density, using Glaso's correlation [59] which shows good agreement with the

measured values. This correlation is represented in Equation 4.14 and it gives the viscosity in mPa·s in terms of the API gravity.

$$\mu_L = 3.141 \cdot 10^{10} \cdot (T - 460)^{-3.444} \cdot [log_{10}(API)]^a \quad \text{Equation 4.14}$$

Where the parameter "a" is calculated with the following temperature correlation:

$$a = 10.313 \cdot [log_{10}(T - 460)] - 36.447 \quad \text{Equation 4.15}$$

With temperature T in ºR.

The molecular diffusivity D_i^L of both solutes H_2 and H_2S to obtain the gas-liquid mass transfer coefficients can be calculated assuming infinite dilution. The diffusivity can be estimated by a Tyn-Calus correlation [62]:

$$D_i^L = 8.93 \cdot 10^{-8} \cdot \frac{v_L^{0.267}}{v_i^{0.433}} \cdot \frac{T}{\mu_L} \quad \text{Equation 4.16}$$

Where T is the temperature in K and μ_L represents the viscosity of the solvent in mPa·s. The molar volume of solute v_i or liquid solvent v_L at its normal boiling temperature can be estimated as published in Perry and Green 1984 [63]:

$$v = 0.285 \cdot v_C^{1.048} \quad \text{Equation 4.17}$$

The critical specific volume v_C of the gaseous compounds H_2 and H_2S can be found tabulated in literature [62], whereas for the liquid components this characteristic can be obtained by using Riazi-Daubert correlation [59]:

$$v_C^m = 7.5214 \cdot 10^{-3} \cdot T_{MeABP}^{0.2896} \cdot d_{15.6}^{-0.7666} \quad \text{Equation 4.18}$$

Where v_C^m is the critical specific volume in ft^3/lb, T_{MeABP} represents the mean average boiling point in ºR and $d_{15.6}$ is the specific gravity at 15.6 ºC that can be obtained using Equation 4.7. The conversion from specific volume to molar volume can be carried out by multiplication by with the average molecular weight of the oil. Because of the complex composition of hydrocarbon mixtures, for this correlation it is considered that organic sulfur compounds have the same density, average boiling point and molecular weight as the whole liquid sample.

The concentrations of the remaining components do not change significantly along the reactor; therefore, they will not be included in the profile modelling.

4.2.1.6 Energy balance

The temperature changes are obtained through all the energy balances present in the reactor. The energy balances for the gas and liquid phases can be expressed as in Equation 4.19 and Equation 4.20, respectively.

$$\rho_G \, c_{P_G} \, u_G \frac{dT}{dz} = U \, S \, (T_r - T) \, + \sum\left[\left(-\Delta H_{R_i}\right)(r_i)\right] \qquad \text{Equation 4.19}$$

$$\rho_L \, c_{P_L} \, u_L \frac{dT}{dz} = U \, S \, (T_r - T) + \sum\left[\left(-\Delta H_{R_i}\right)(r_i)\right] \qquad \text{Equation 4.20}$$

A global energy balance can be obtained with the addition of both gas and liquid contributions. The solid phase is not considered in the energy balance. In the literature reactor model, [24] the hydrotreating reactor is assumed as adiabatic when working on an industrial scale. The global balance is given by the following equation.

$$\frac{dT}{dz} = \sum\left[\left(-\Delta H_{R_i}\right)(r_i)\right] \cdot \frac{\epsilon_L}{u_G \, \rho_G \, c_{P_G} \epsilon_G + u_L \, \rho_L \, c_{P_L} \epsilon_L} \qquad \text{Equation 4.21}$$

4.2.2 Kinetic model

In this section two different kinetic models are formulated. Both models classify the compounds in the feed in lumps.

4.2.2.1 Model A. High order kinetic models

This model is based on a classification of the sulfur compounds in 4 lumps that best describes the feedstock: mercaptans, thiophenes, dibenzothiophenes (DBT) and alkyl dibenzothiophenes (alkyl DBT). Nitrogen compounds are classified in one lump with acridine as reference molecule.

The kinetic expression for the nitrogen lump was assumed as a first order reaction rate depending on both reactants (H_2 and ‘i' nitrogen compound). Mercaptans are highly

reactive by which the same type of expression was applied to model this reaction as follows:

$$r_i = k_i\, C_N\, C_{H_2} \qquad \text{Equation 4.22}$$

The kinetic expression described in Equation 4.23 assumes competitive adsorption on the same catalytic sites between the reactant "i" (thiophenes, DBT, and alkyl DBT in each case), H_2 H_2S and component:

$$r_i = \frac{k_i K_i (C_i)^p K_{H_2} (C_{H_2})^q}{\left(1 + K_{H_2S} C_{H_2S} + K_{H_2} C_{H_2} + K_i C_i\right)^3} \qquad \text{Equation 4.23}$$

In Figure 4.2 a schematic description of the reactor model and the considered hydrotreating reactions in this model are illustrated.

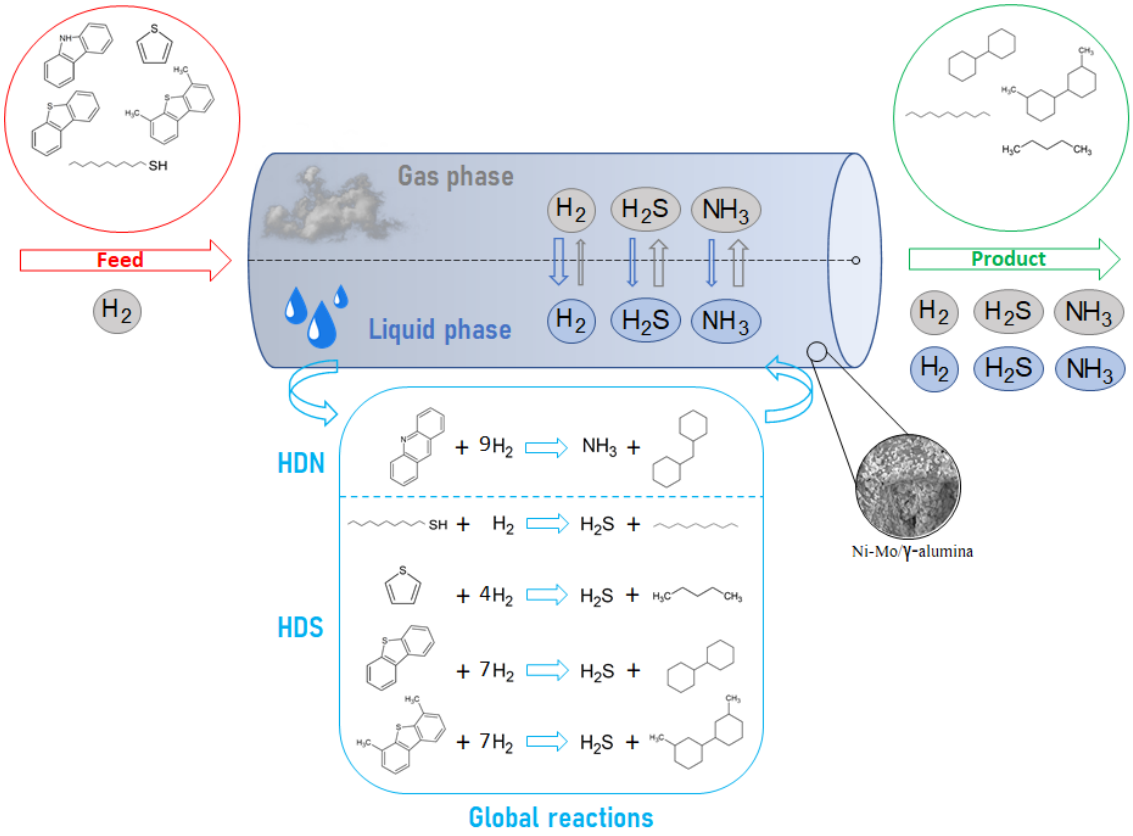

Figure 4.2 Model description with global hydrotreating reactions.

The reaction rate constants are calculated following the Arrhenius law:

$$k = A \cdot e^{-\frac{E_a}{RT}} \qquad \text{Equation 4.24}$$

Where A is the pre-exponential factor and E_a the activation energy.

The equilibrium adsorption constants, K_i , are calculated via Van't Hoff equation:

$$K_i = e^{\frac{\Delta S_{ads\,i}}{R}} \cdot e^{-\frac{\Delta H_{ads\,i}}{RT}} = B_i \cdot e^{-\frac{\Delta H_{ads\,i}}{RT}} \qquad \text{Equation 4.25}$$

Where ΔH_{ads_i} and $\Delta S_{ads\,i}$ are the enthalpy adsorption and the entropy of adsorption of reaction component i. B_i is a pre-exponential factor which works as an analogous to the one in the Arrhenius equation. Note that in the competitive adsorption not only the reactants are considered, but also the inhibition effects of the hydrogen sulphide produced and the hydrogen that is reacting.

The theoretical conversion inside the reactor is obtained using Equation 4.26. This can be applied for both HDS and HDN reactions.

$$X_i = \frac{C_{i_0} - C_i}{C_{i_0}} \qquad \text{Equation 4.26}$$

Where C_{i_0} is the initial concentration of component i in the feedstock and C_i is the concentration of the component 'i' in the product.

4.2.2.2 Model B. Two active sites for HDS

Two catalytic active sites were considered in this second kinetic model: σ-sites for hydrogenolysis reactions and τ-sites for hydrogenation.

The total nitrogen content was modelled in one lump again, with acridine as the reference molecule. The kinetic expression was proposed following a law of mass action approach:

$$r_{HDN} = k_{HDN}\, C_N^{1.5}\, C_{H_2}^{1.5} \qquad \text{Equation 4.27}$$

The mercaptans HDS reaction was described as a reversible reaction, as depicted graphically in Figure 3. According to Ghosh et al. [64] the forward reaction dominates for the most part.

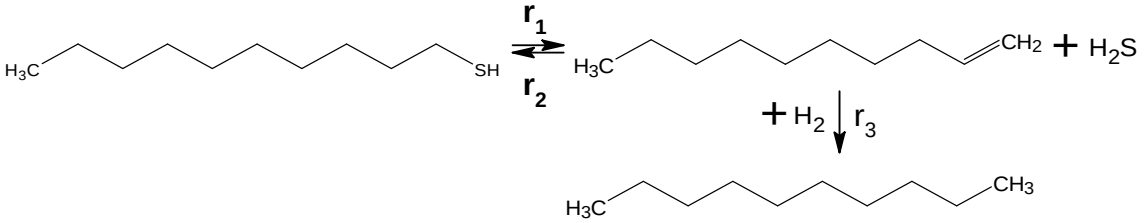

Figure 4.3 Mercaptan HDS reaction network.

$$r_1 = k_1\, C_{Mercaptans}$$ Equation 4.28

$$r_2 = k_2\, C_{Olefine}\, C_{H_2S}$$ Equation 4.29

$$r_3 = k_1\, C_{Olefine}$$ Equation 4.30

Thiophenes were modelled with an intermediate step where the thiophene is hydrogenated to tetrahydrothiophene (TT), as shown in Figure 4.4. Hydrogenolysis and hydrogenation were assumed to occur in different catalytic sites and, therefore, two independent reaction rates are required [17][30].

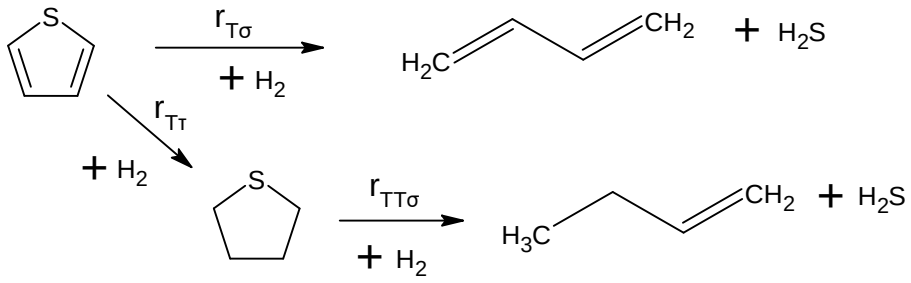

Figure 4.4 Thiophene HDS reaction network.

$$r_{T\sigma} = \frac{k_{T\sigma}\, C_T\, C_{H_2}}{1 + K_T C_T + K_{H_2S} C_{H_2S}}$$ Equation 4.31

$$r_{T\tau} = k_{T\tau}\, C_T\, C_{H_2}$$ Equation 4.32

$$r_{TT_\sigma} = \frac{k_{T_\sigma}\, C_{TT}\, C_{H_2}}{1 + K_T C_T + K_{H_2S} C_{H_2S}}$$ Equation 4.33

Dibenzohiophenes (DBT) were modelled following the same reaction scheme, with tetrahydrodibenzothiophene (THDBT) as intermediate reaction specie, as described graphically in Figure 4.5. Kinetic expressions for hydrogenolysis and hydrogenation were taken from previous works [65].

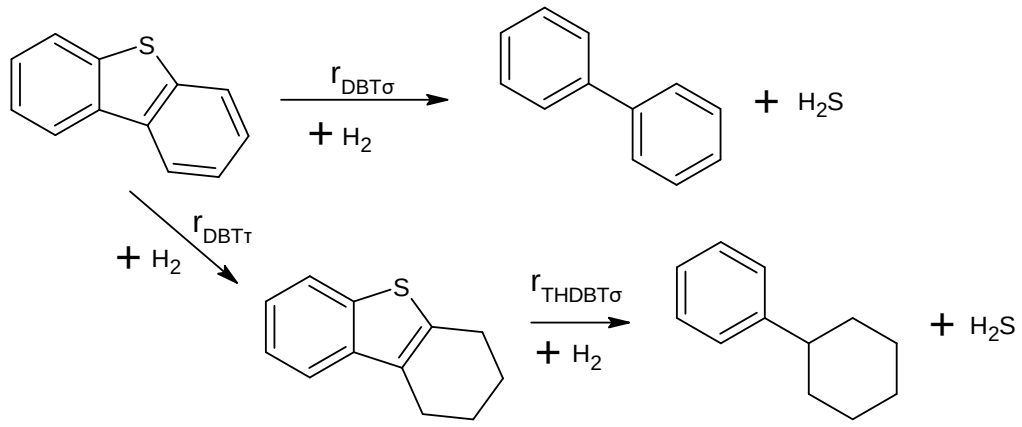

Figure 4.5 Dibenzothiophene HDS reaction network.

$$r_{DBT\sigma} = \frac{k_{DBT\sigma}\, K_{DBT\sigma}\, K_{H_2\sigma}\, C_{DBT}\, C_{H_2}}{(1 + K_{DBT\sigma}\, C_{DBT} + \sqrt{K_{H_2\sigma} C_{H_2}} + K_{H_2S}\frac{C_{H_2S}}{C_{H_2}})} \qquad \text{Equation 4.34}$$

$$r_{DBT\tau} = \frac{k_{DBT\tau}\, K_{DBT\tau}\, C_{DBT}\, C_{H_2}}{(1 + K_{DBT\tau} C_{DBT})^3} \qquad \text{Equation 4.35}$$

Alkyl dibenzothiophenes were modelled using the same kinetic expressions as the case for DBT, but in this case using 4,6-DM-DBT as a reference molecule. The 4,6-DM-DBT reaction network path is depicted in Figure 4.6.

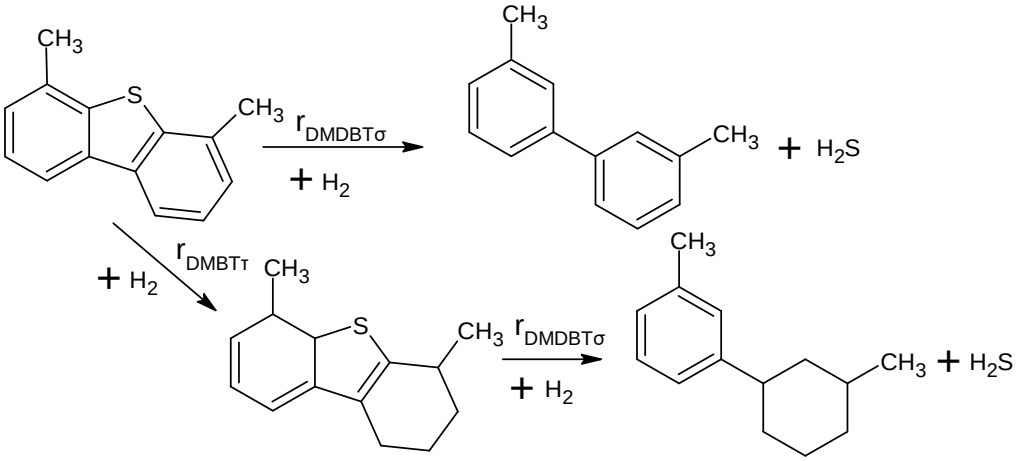

Figure 4.6 4,6-DM-DBT HDS reaction network.

4.2.3 Model resolution

With the appropriate reactor configuration and the equations described in the methodology section (from Equation 4.1 to Equation 4.21), the model was implemented using Python Programming Language.

The system of ODE's (ordinary differential equations) was solved using the integrator 'lsoda', which switches automatically between stiff and non-stiff methods automatically choosing the appropriate one.

4.3 Parameter estimation

Kinetic parameters are determined by solving the following optimization problem:

$$\min_{\lambda \epsilon X} f(\lambda)$$

Where $f(\lambda)$ is the objective function and λ is the estimated parameter vector bounded by X. The optimization algorithm was employed to estimate the vector of parameters λ that minimizes the objective function. The objective function is the sum of squared errors (SSE) between the experimental compositions in the product and the compositions calculated by the simulation:

$$f(\lambda) = \sum_{i=1}^{N_{Lumps}} \sum_{j=1}^{N_{Experiments}} \left[C_{exp}(i,j) - C_{sim}(i,j)\right]^2 \qquad \text{Equation 4.36}$$

This type of unconstrained optimization problems was addressed with the Nelder-Mead simplex algorithm that is based on direct search for solving [66].

The Nelder-Mead algorithm minimize a function of n variables, which depends on the comparison of function values at the (n + 1) vertices of a general simplex, followed by the replacement of the vertex with the highest value by another point. The simplex adapts itself to the local landscape, and contracts on to the final minimum. This method is shown to be effective and computationally compact [67].

In some cases, Nelder-Mead algorithm might be inefficient at finding the global minimum in a high dimensional problem. This issue can be fixed using an improved version called Adaptive Nelder-Mead Simplex (ANMS) method which proved to perform better in large dimensional problems [66]. Therefore, this improved method is the one that will be implemented for solving the optimization problem.

4.4 Model assessment

In order to evaluate the accuracy of the model, different procedures can be carried out. One of them is to analyse the significance of the kinetic parameters from a chemical

engineering perspective, evaluating if the magnitude orders are reasonable and the discrepancies between the values obtained for each lump.

4.4.1 Parity diagram

A parity diagram will be included as part of the methodology in this work. The parity diagram consists in plotting the experimental compositions against the ones obtained in the simulated reactor. These compositions are desired to be in the line y=x as much as possible, which means that the model predicts exactly the product composition.

4.4.2 Residual analysis

The residuals, also called residues or rest values, are defined as the difference between the value calculated with the aid of the model that has been fitted to the data and the observed values for the dependent variable. Thus, the residuals express the quantity in the observation outcome that cannot be described by the model.

$$e_{ij} = y_{ij}^{model} - y_{ij}^{experimental} \qquad \text{Equation 4.37}$$

In this case, the dependent variable y_{ij} is the concentration in the product of the lump i at the experiment j, and the value of $\hat{y}_{ij}$ is the composition that the model predicted for that experiment.

If the used model is valid for some specific dependent variable, the distribution of the residuals is expected to represent an aleatory distribution around zero (homoscedasticity). If the residual plot is biased or represent a strong pattern, it means the considered hypothesis in the model may be inadequate.

5. Results

5.1 Data set analysis

From the feedstock data collected in Table 4.1 it can be observed that CGO has a higher content in both nitrogen and sulfur compounds than DF. Mercaptans and thiophenes are the compounds lumps with more sulfur content in the feedstocks, representing about 90% of the total content.

The HDS (left) and HDN (right) conversions for each processed feed is graphically described in Figures 5.1, 5.2 and 5.3 respectively. For each condition of reaction temperature, pressure and LHSV the conversion is illustrated in a color/size scale.

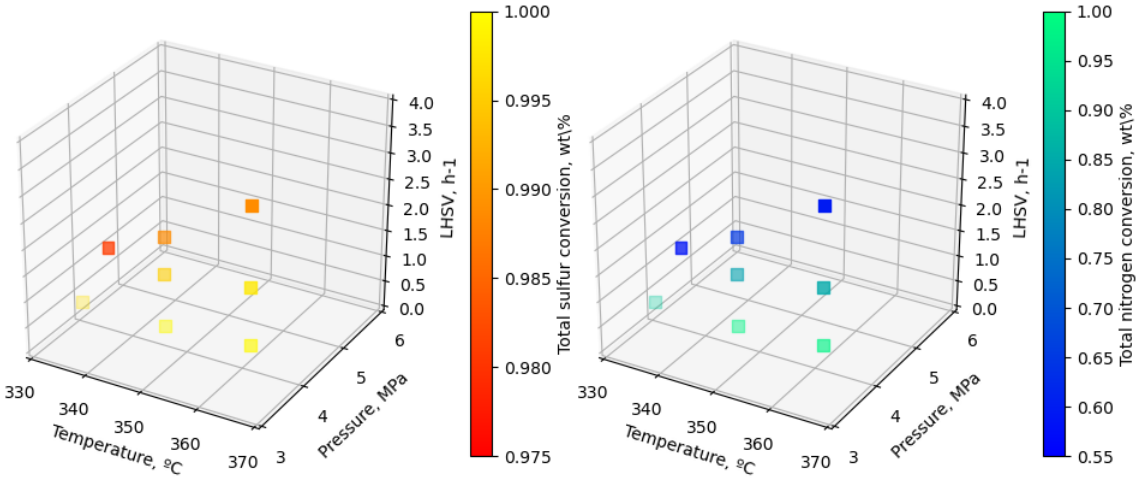

Figure 5.1 Conversions of DF hydrotreating at different process conditions.

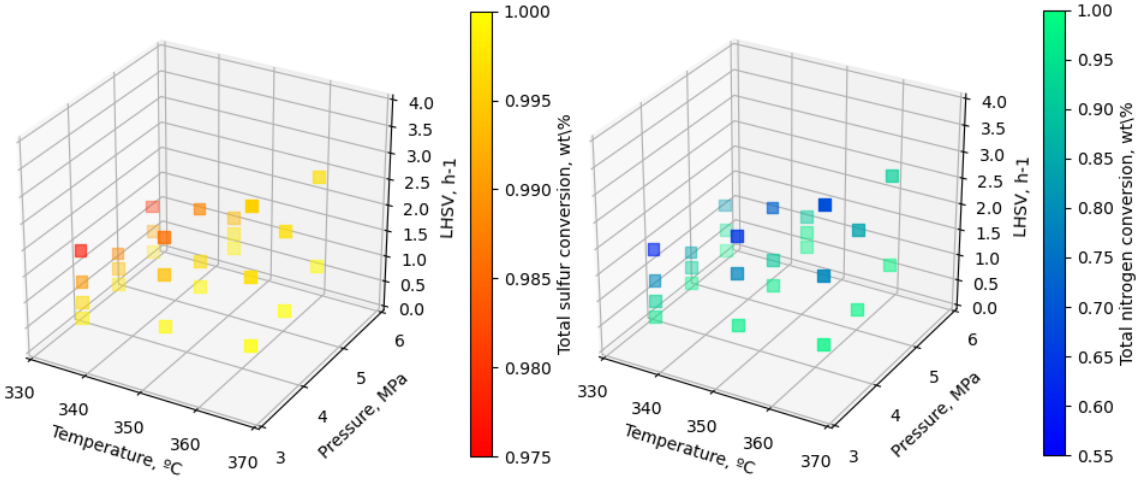

Figure 5.2 Conversions of DF+15%CGO hydrotreating at different process conditions.

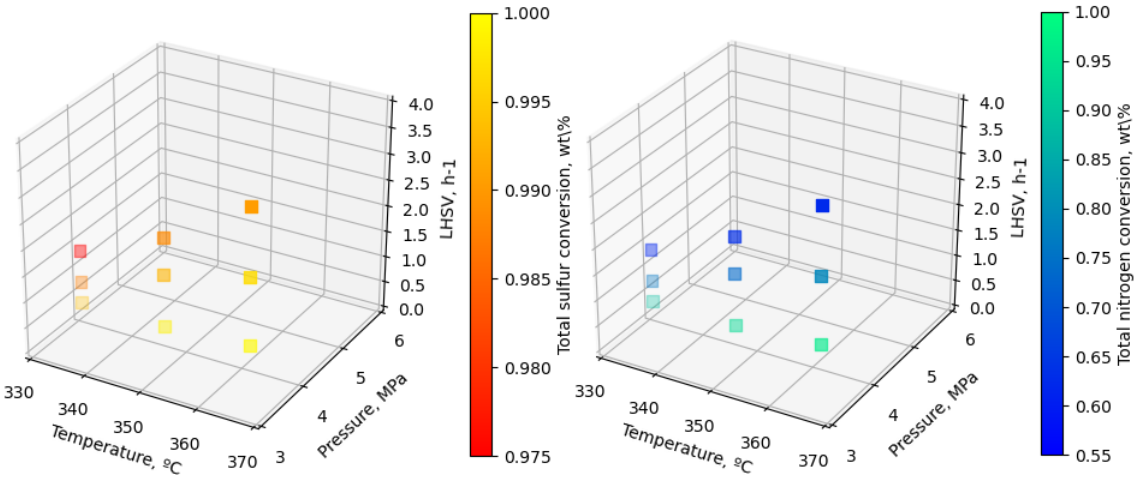

Figure 5.3 Conversions of DF+30%CGO hydrotreating at different process conditions.

Some qualitative conclusions can be drawn from these figures. On the one hand, the highest conversions were achieved at the highest temperatures and the lowest LHSV, which corresponds with the expected behaviour. The temperature effect on the conversion predominates over the rest of the conditions.

The experiments were carried out at different operating conditions. Some of the experiments were repeated using the same conditions and different values in the product composition were obtained. Table 5.1 shows the standard deviations of these experiments.

Table 5.1 Standard deviations in repeated experiments

Total S, ppm	Total N, ppm	Mercaptans, ppm	Thiophenes, ppm	DBT, ppm	Alkyl DBT, ppm
42.69	10.72	8.61	26.35	7.63	7.72

5.2 Model A

In this section, the results obtained in the first lumped kinetic model are presented. With the experimental values of Table 4.1 and Table 4.2 and the new kinetic expressions described in Equation 4.22 and 4.23, the kinetic parameters and adsorption constants were determined using the procedure described in section 4.2.

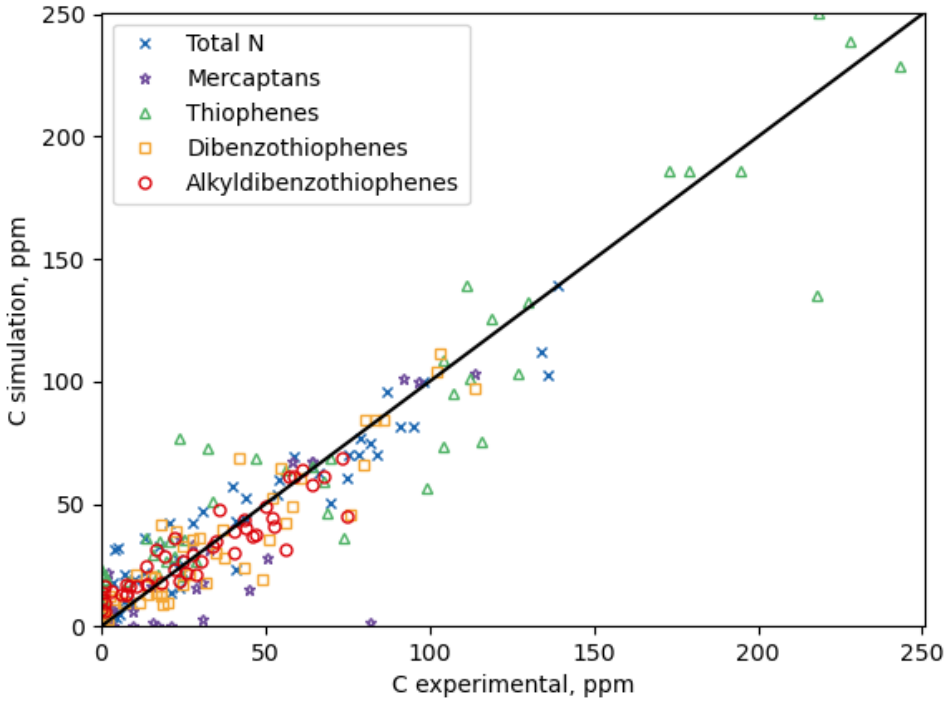

Figure 5.4 Comparison between experimental data and calculated mass compositions.

The Pearson correlation coefficient for the parity plot of all predictions is r = 0.941. Tin the simulation 66% of the experimental points li in the range covered by the range [-σ,+ σ] where σ is the standard deviation calculated from the results of repeated experiments. The lumps whose conversion is better described by the model is the thiophenes, with 81% of the experimental points simulated into the range of experimental uncertainty. Table 5.2 collects the percentages of success predictions with this model A on the lump conversions. Looking at these results, when increasing the molecular weight, the predictions are less successful, as with the DBT and Alkyl DBT compounds.

Table 5.2 Percentages of success in the conversion predictions.

Total S, %	Total N, %	Mercaptans, %	Thiophenes, %	DBT, %	Alkyl DBT, %
70.2	63.8	68.1	80.1	57.4	61.7

Figure 5.6 represents the experimental points of total sulfur and total nitrogen concentrations that fit in the range of the standard deviation. The 70% of the total sulfur points lied inside the given uncertainty, whereas in case of nitrogen 64% of the points were properly predicted.

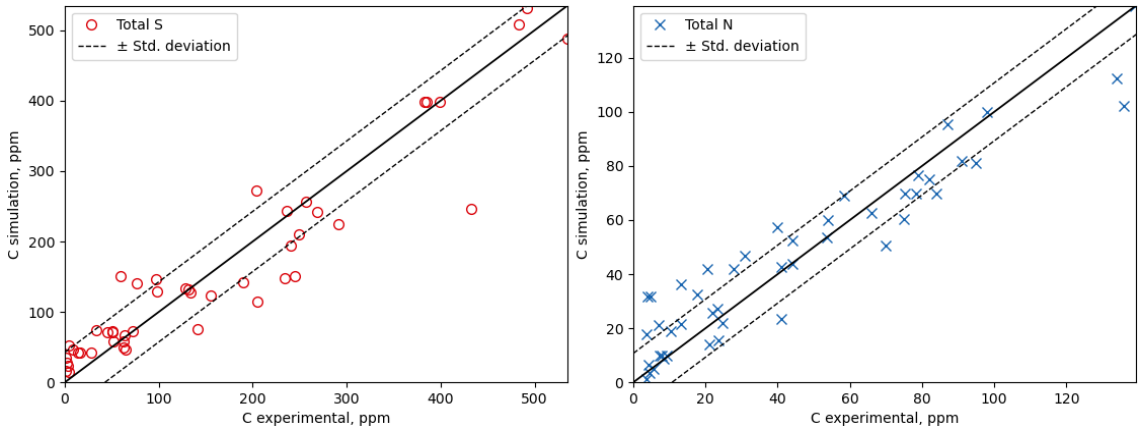

Figure 5.5 Experimental and simulated points of total sulfur and total nitrogen.

Table 5.3 shows the kinetic and adsorption parameter values determined as a result of the applied parameter optimization procedure. It also includes the apparent reaction constants at 350ºC. Mercaptans, which is the f are lower than the values determined for thiophenes, in an opposed behavior as would be expected. Mercaptans showed lower rate constants than expected, since it is the most reactive compound. The rate apparent constants for thiophenes DBT and alkyl DBT adopted similar values, being alkyl DBT the lump with the lowest value. The kinetic parameters are higher than the rest, which was not expected due to its refractory properties. These parameters are balanced with the very low adsorption constants these compounds obtained, which value also participates in the reaction rate equation.

Table 5.3 Kinetic parameters and adsorption constants

	A	**Ea, J/mol**	**B**	**Hads, J/mol**	**k_{app} (350°C)**
Total N	1.51E+17	1.24E+05	-	-	5.83E+06
Mercaptans	9.58E+17	1.52E+05	-	-	1.57E+05
Thiophenes	2.95E+15	8.35E+04	5.41E+03	5.90E+04	1.80E+07
DBT	2.52E+17	1.12E+05	2.75E+03	4.86E+04	2.34E+07
Alkyl DBT	6.57E+21	1.05E+05	1.83E-06	9.69E+01	1.75E+07
H2	-	-	1.11E+03	6.11E+04	-
SH2	-	-	5.46E+04	6.34E+04	-

The orders of reaction obtained by the model were p = 1.51 (for sulfur compounds) and q = 0.41 (for H_2). A similar pseudo reaction order value (0.45) was found for hydrogen reactant in a previous HDS research [15].

In Figure 5.6 the residual graphs of total nitrogen against the operating variables are illustrated. It can be observed that the residual values seem to be moderately correlated with the LHSV variable. A slightly similar behaviour was observed when plotting the sulfur lump residuals as the thiophenes (Figure 5.7) for instance. This fact can explain that the effect of the LHSV on the conversions was not as well predicted by the model as for the rest of the operating variables.

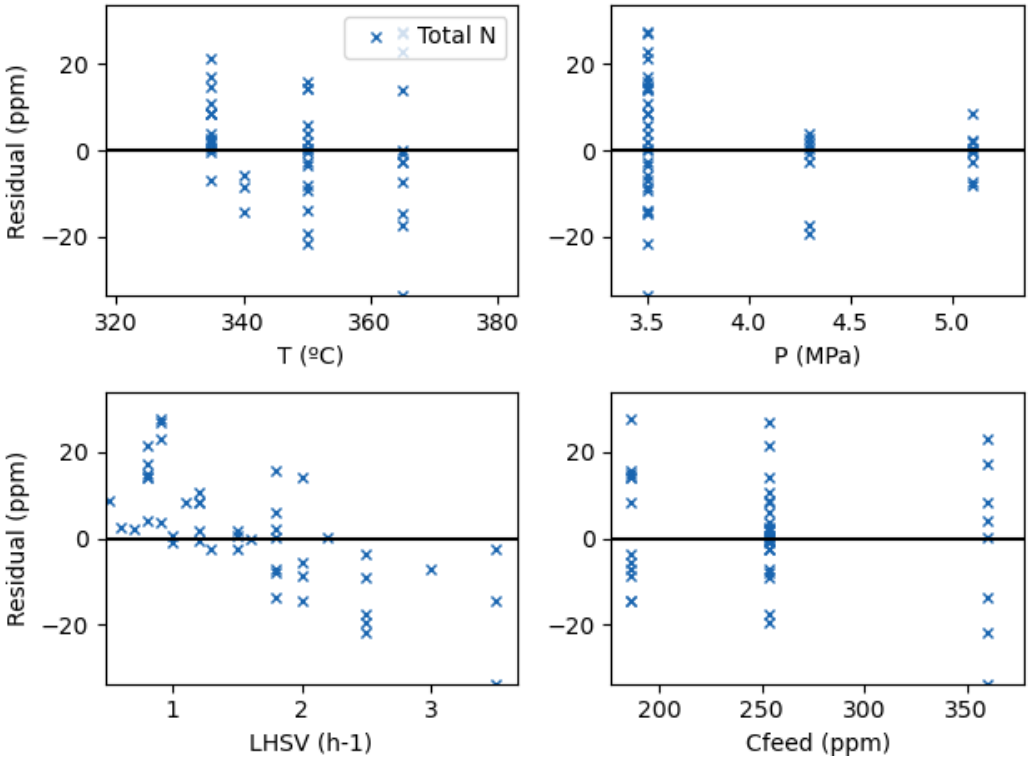

Figure 5.6 Residual values of total nitrogen concentrations in the product.

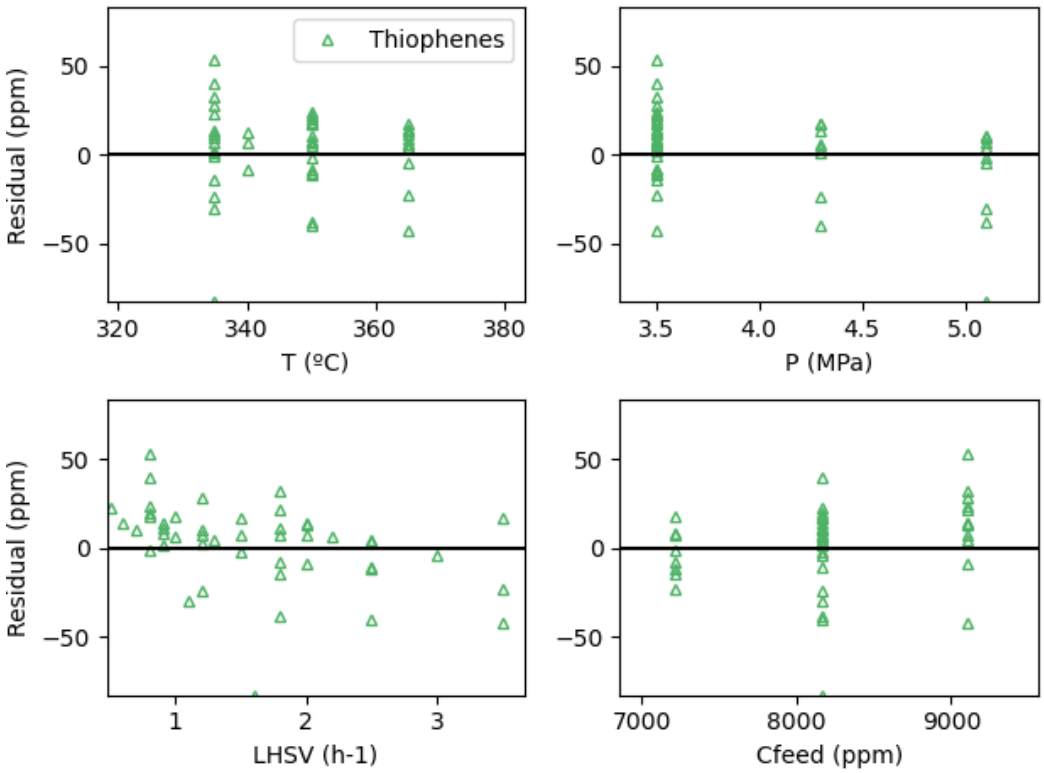

Figure 5.7 Residual values of thiophene concentrations in the product.

5.3 Model B

In this section, the results obtained in the second lumped kinetic model are presented. With the experimental values of Table 5.2 and Table 5.3 and the new kinetic expressions from Eq. 4.27 to Eq. 4.30, the kinetic parameters and adsorption constants were determined again using the procedure described in section 4.2.

A comparison between experimental and calculated mass compositions in the product is shown in Figure 5.8.

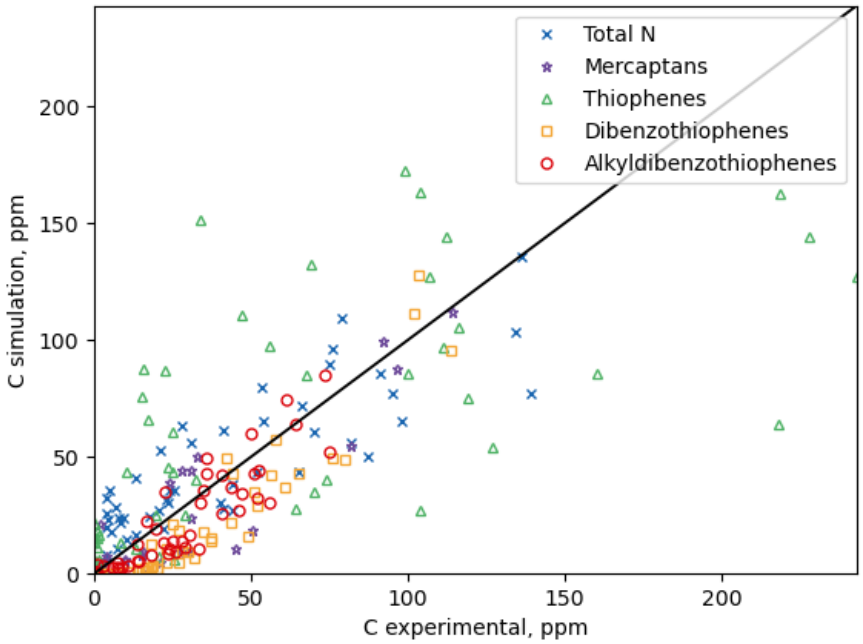

Figure 5.8 Comparison between experimental data and calculated mass compositions.

The Pearson correlation coefficient for the parity plot is r = 0.841. In this simulation only 47% lie in the range of the experimental uncertainty. The better described lumps in this model are the mercaptans, with 72% of the experimental points simulated in the range of experimental uncertainty. Table 5.4 collects the percentages of success predictions with this model A on the lump conversions.

Table 5.4 Percentages of success in the conversion predictions.

Total S, %	Total N, %	Mercaptans, %	Thiophenes, %	DBT, %	Alkyl DBT, %
68.1	38.3	72.3	48.9	29.8	46.8

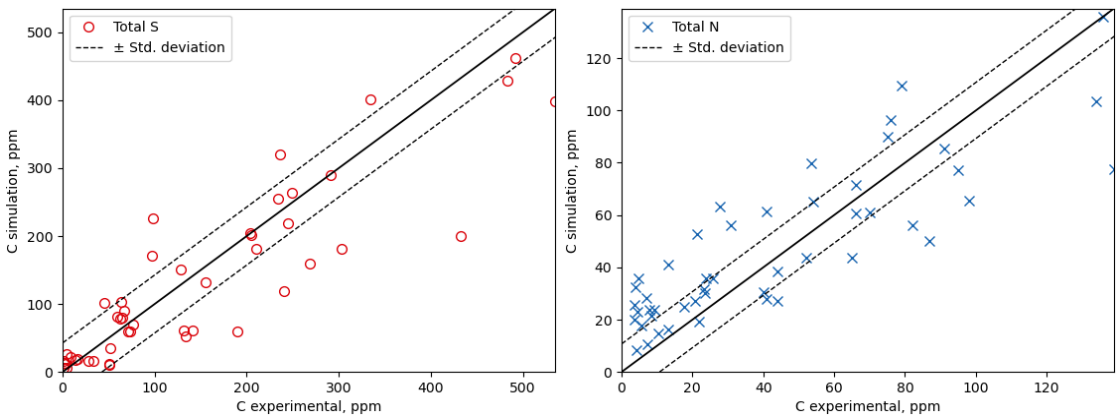

Figure 5.9 Experimental and simulated points of total sulfur and total nitrogen.

Figure 5.9 illustrates the experimental points of total sulfur and total nitrogen. It can be observed that the previous model attempted to describe better the HDS and HDN conversions than the current model. In Figure 5.10 the residual graphs of total nitrogen against the operating variables are illustrated. In this case, the residuals tend to be correlated with the temperature, which is not the behavior desired. Looking at the residuals for the rest of the lumps a similar correlation appears, such as the case of the thiophenes (Figure 5.11), which indicates that this model might be inadequate.

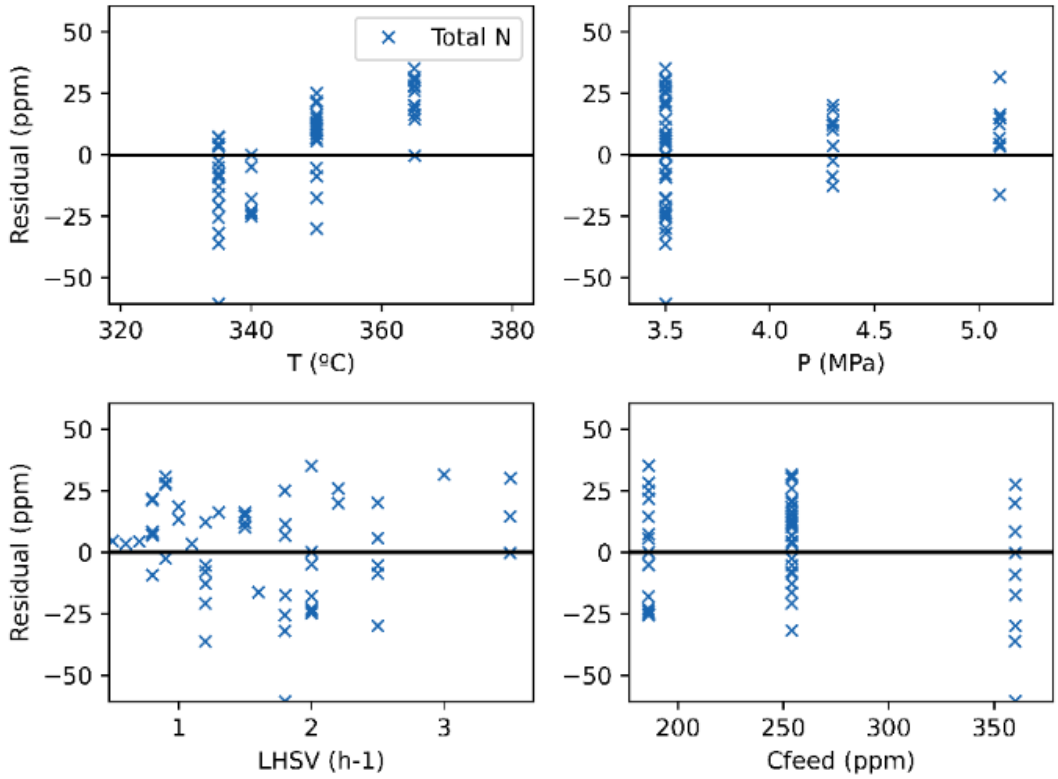

Figure 5.10 Residual values of total nitrogen concentrations in the product.

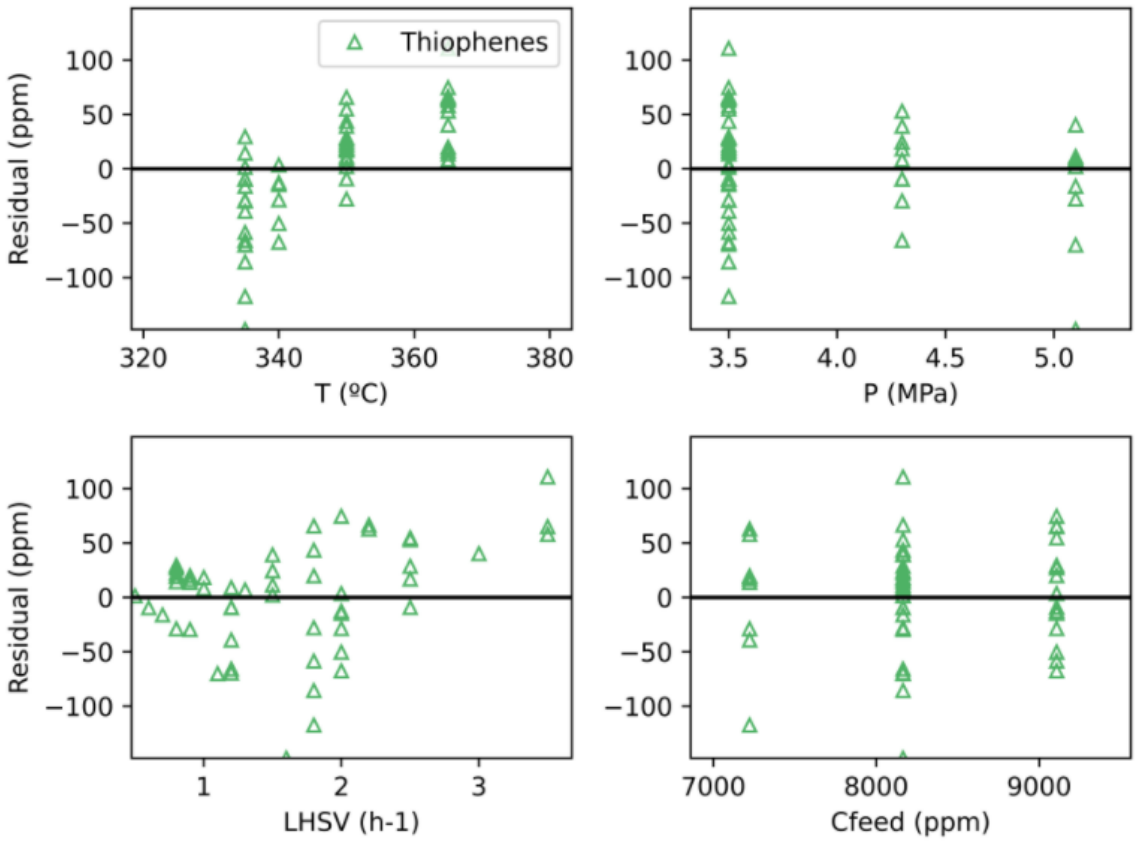

Figure 5.11 Residual values of thiophenes concentrations in the product.

Comparing the results obtained in this model with those obtained in the first model, it can be concluded that better predictions in the HDS and HDN conversions were obtained using the global kinetics described in model A.

6. Conclusions and future work

Two different kinetic approaches were proposed in the hydrotreating of medium oil cuts. The first model was based on global kinetics for sulfur and nitrogen compounds. The second model was based on a more detailed kinetic formulation that considers different active sites for the hydrogenolysis and the hydrogenation reaction of sulfur compounds, reversibility in the mercaptans reaction and higher order for nitrogen reactions.

Better predictions were obtained with the first model in terms of the number of Pearson correlation coefficient of the regression line in the global parity plot and the number of points predicted by the model in the expected uncertainty range. In general, the apparent reaction rates for all the lumps were found reasonable considering the expected reactivity of the molecule.

The temperature effect on the conversion predominated over the rest of the conditions. A strong correlation with LHSV was observed in the residuals of most of the variables which indicate a strong influence on this variable on the final conversion that must be better addressed by the model.

Lumped kinetic models proved to be very efficient since the reduction in the kinetic parameters is very large when dealing with complex feedstocks. The competitive adsorption between H_2, H_2S and the sulfur compounds was successfully captured using a Langmuir-Hinshelwood formalism. Mercaptans HDS was better captured in the second model considering a reversible reaction. In general, low molecular-weight components are more accurately predicted by the proposed model.

The effects of the LHSV on the conversion need to be better addressed in the model. These effects were tried to be captured in the second model including a correlation but failed in giving better conversion predictions. Better results could be obtained if adding more variability in the feedstocks.

As future work, a different kinetic approach could be proposed for the hydrotreating medium oil cuts, for instance using the Single-Event MicroKinetics (SEMK) methodology that was described in section 3.1.2 and then, compare the results with the model proposed in this work.

7. References

[1] M. Mohammadpoor and F. Torabi, “Big Data analytics in oil and gas industry: An emerging trend,” *Petroleum*, 2018, doi: https://doi.org/10.1016/j.petlm.2018.11.001.

[2] E. Iplik, I. Aslanidou, and K. Kyprianidis, “Hydrocracking: A Perspective towards Digitalization,” *Sustainability*, vol. 12, no. 17, p. 7058, Aug. 2020, doi: 10.3390/su12177058.

[3] M. A. Fahim, T. A. Alsahhaf, and A. Elkilani, “Chapter 8 - Fluidised Catalytic Cracking,” M. A. Fahim, T. A. Alsahhaf, and A. B. T.-F. of P. R. Elkilani, Eds. Amsterdam: Elsevier, 2010, pp. 199–235.

[4] M. I. Ahmad, “Integrated and Multi-Period design of Diesel Hydrotreating Process,” 2009.

[5] P. J. Becker, B. Celse, D. Guillaume, H. Dulot, and V. Costa, “Hydrotreatment modeling for a variety of VGO feedstocks: A continuous lumping approach,” *Fuel*, vol. 139, pp. 133–143, 2015, doi: https://doi.org/10.1016/j.fuel.2014.08.032.

[6] N. Bergvall, L. Sandström, F. Weiland, and O. G. W. Öhrman, “Corefining of Fast Pyrolysis Bio-Oil with Vacuum Residue and Vacuum Gas Oil in a Continuous Slurry Hydrocracking Process,” *Energy & Fuels*, vol. 34, no. 7, pp. 8452–8465, Jul. 2020, doi: 10.1021/acs.energyfuels.0c01322.

[7] J. G. Speight, “Chapter 4 - Effects in Refining,” J. G. B. T.-H. A. C. Speight, Ed. Boston: Gulf Professional Publishing, 2014, pp. 77–109.

[8] X. Liang, Y. Liu, and L. Kang, “Retrofit and optimisation for a vacuum gas oil hydrotreating system based on exergy load distribution analysis,” *Int. J. Exergy*, vol. 21, p. 347, Jan. 2016, doi: 10.1504/IJEX.2016.080066.

[9] S. Vedachalam, A. Dalai, and J. Adjaye, “The effect of phosphorus on hydrotreating property of NiMo/γ-Al 2O 3 nitride catalyst,” *Appl. Catal. A-general - APPL CATAL A-GEN*, vol. 335, pp. 204–210, Feb. 2008, doi: 10.1016/j.apcata.2007.11.024.

[10] J. G. Speight and N. S. El-Gendy, “Chapter 7 - Biocatalytic Denitrogenation,” J. G. Speight and N. S. B. T.-I. to P. B. El-Gendy, Eds. Boston: Gulf Professional Publishing, 2018, pp. 229–258.

[11] J. G. Speight, “Chapter 8 - Hydrotreating and Desulfurization,” J. G. B. T.-T. R. of the F. Speight, Ed. Boston: William Andrew Publishing, 2011, pp. 237–273.

[12] N. P. Cheremisinoff and P. Rosenfeld, “Chapter 1 - The petroleum industry,” N. P. Cheremisinoff and P. B. T.-H. of P. P. and C. P.-B. P. in T. P. I. Rosenfeld, Eds. Oxford: William Andrew Publishing, 2009, pp. 1–97.

[13] R. Prins, M. Egorova, A. Röthlisberger, Y. Zhao, N. Sivasankar, and P. Kukula, “Mechanisms of hydrodesulfurization and hydrodenitrogenation,” *Catal. Today*, vol. 111, no. 1, pp. 84–93, 2006, doi: https://doi.org/10.1016/j.cattod.2005.10.008.

[14] S. K. Bej, A. K. Dalai, and J. Adjaye, “Comparison of Hydrodenitrogenation of Basic and Nonbasic Nitrogen Compounds Present in Oil Sands Derived Heavy Gas Oil,” *Energy & Fuels*, vol. 15, no. 2, pp. 377–383, Mar. 2001, doi: 10.1021/ef0001484.

[15] M. A. Rodríguez and J. Ancheyta, “Modeling of Hydrodesulfurization (HDS), Hydrodenitrogenation (HDN), and the Hydrogenation of Aromatics (HDA) in a Vacuum Gas Oil Hydrotreater,” *Energy & Fuels*, vol. 18, no. 3, pp. 789–794, May 2004, doi: 10.1021/ef030172s.

[16] N. Charon-Revellin, H. Dulot, C. Lopez-Garcia, and J. Jose, “Kinetic Modeling of Vacuum Gas Oil Hydrotreatment using a Molecular Reconstruction Approach,” *Oil Gas Sci. Technol.*, vol. 66, pp. 479–490, May 2010, doi: 10.2516/ogst/2010005.

[17] M. J. Girgis and B. C. Gates, “Reactivities, reaction networks, and kinetics in high-pressure catalytic hydroprocessing,” *Ind. Eng. Chem. Res.*, vol. 30, no. 9, pp. 2021–2058, Sep. 1991, doi: 10.1021/ie00057a001.

[18] P. E. Boahene, “Effect of pore diameter variation of FeW/SBA-15 supported catalysts on hydrotreating of heavy gas oil from Athabasca bitumen,” 2011.

[19] C. S. Raghuveer, “Hydrodenitrogenation kinetics according to single-event

methodology," 2016.

[20] M.-T. Nguyen, M. Tayakout-Fayolle, F. Chainet, G. D. Pirngruber, and C. Geantet, "Use of kinetic modeling for investigating support acidity effects of NiMo sulfide catalysts on quinoline hydrodenitrogenation," *Appl. Catal. A Gen.*, vol. 530, pp. 132–144, 2017, doi: https://doi.org/10.1016/j.apcata.2016.11.015.

[21] M.-T. Nguyen, M. Tayakout-Fayolle, G. D. Pirngruber, F. Chainet, and C. Geantet, "Kinetic Modeling of Quinoline Hydrodenitrogenation over a NiMo(P)/Al2O3 Catalyst in a Batch Reactor," *Ind. Eng. Chem. Res.*, vol. 54, no. 38, pp. 9278–9288, Sep. 2015, doi: 10.1021/acs.iecr.5b02175.

[22] R. A. Sánchez-Delgado, Ed., "Hydrodesulfurization and Hydrodenitrogenation BT - Organometallic Modeling of the Hydrodesulfurization and Hydrodenitrogenation Reactions," Dordrecht: Springer Netherlands, 2002, pp. 1–34.

[23] M. A. Fahim, T. A. Alsahhaf, and A. Elkilani, "Chapter 2 - Refinery Feedstocks and Products," M. A. Fahim, T. A. Alsahhaf, and A. B. T.-F. of P. R. Elkilani, Eds. Amsterdam: Elsevier, 2010, pp. 11–31.

[24] H. Korsten and U. Hoffmann, "Three-phase reactor model for hydrotreating in pilot trickle-bed reactors," *AIChE J.*, vol. 42, no. 5, pp. 1350–1360, May 1996, doi: 10.1002/aic.690420515.

[25] I. Mochida and K. H. Choi, "An overview of hydrodesulfurization and hydrodenitrogenation," *J. Japan Pet. Inst.*, vol. 47, no. 3, pp. 145–163, 2004, doi: 10.1627/jpi.47.145.

[26] S. Boichenko and M. Zakharchuk, *AVIATION FUELS AND LUBRICANTS*. 2012.

[27] W. Bensch, "7.12 - Hydrotreating: Removal of Sulfur from Crude Oil Fractions with Sulfide Catalysts," J. Reedijk and K. B. T.-C. I. C. I. I. (Second E. Poeppelmeier, Eds. Amsterdam: Elsevier, 2013, pp. 287–321.

[28] J. V Lauritsen *et al.*, "Hydrodesulfurization reaction pathways on MoS2 nanoclusters revealed by scanning tunneling microscopy," *J. Catal.*, vol. 224, no.

1, pp. 94–106, 2004, doi: https://doi.org/10.1016/j.jcat.2004.02.009.

[29] F. Richard, T. Boita, and G. Pérot, “Reaction mechanism of 4,6-dimethyldibenzothiophene desulfurization over sulfided NiMoP/Al2O3-zeolite catalysts,” *Appl. Catal. A Gen.*, vol. 320, pp. 69–79, 2007, doi: https://doi.org/10.1016/j.apcata.2006.12.014.

[30] I. A. Van Parijs and G. F. Froment, “Kinetics of hydrodesulfurization on a cobalt-molybdenum/.gamma.-alumina catalyst. 1. Kinetics of the hydrogenolysis of thiophene,” *Ind. Eng. Chem. Prod. Res. Dev.*, vol. 25, no. 3, pp. 431–436, Sep. 1986, doi: 10.1021/i300023a011.

[31] I. A. Van Parijs, L. H. Hosten, and G. F. Froment, “Kinetics of the hydrodesulfurization on a cobalt-molybdenum/.gamma.-alumina catalyst. 2. Kinetics of the hydrogenolysis of benzothiophene,” *Ind. Eng. Chem. Prod. Res. Dev.*, vol. 25, no. 3, pp. 437–443, Sep. 1986, doi: 10.1021/i300023a012.

[32] V. Vanrysselberghe and G. F. Froment, “Hydrodesulfurization of Dibenzothiophene on a CoMo/Al2O3 Catalyst: Reaction Network and Kinetics,” *Ind. Eng. Chem. Res.*, vol. 35, no. 10, pp. 3311–3318, Jan. 1996, doi: 10.1021/ie960099b.

[33] M. Bhaskar, G. Valavarasu, B. Sairam, K. S. Balaraman, and K. Balu, “Three-Phase Reactor Model to Simulate the Performance of Pilot-Plant and Industrial Trickle-Bed Reactors Sustaining Hydrotreating Reactions,” *Ind. Eng. Chem. Res.*, vol. 43, no. 21, pp. 6654–6669, Oct. 2004, doi: 10.1021/ie049642b.

[34] Z. Chen *et al.*, “Molecular-level kinetic modelling of fluid catalytic cracking slurry oil hydrotreating,” *Chem. Eng. Sci.*, vol. 195, pp. 619–630, 2019, doi: https://doi.org/10.1016/j.ces.2018.10.007.

[35] M. Bhaskar, G. Valavarasu, A. Meenakshisundaram, and K. Balaraman, “Application of a three phase heterogeneous model to analyse the performance of a pilot plant trickle bed reactor,” *Pet. Sci. Technol. - PET SCI TECHNOL*, vol. 20, pp. 251–268, Jan. 2002, doi: 10.1081/LFT-120002098.

[36] M. Mapiour, S. Vedachalam, A. Dalai, and J. Adjaye, “Effects of the operating variables on hydrotreating of heavy gas oil: Experimental, modeling, and kinetic studies,” *Fuel*, vol. 89, pp. 2536–2543, Sep. 2010, doi: 10.1016/j.fuel.2010.02.024.

[37] E. Rodríguez, G. Félix, J. Ancheyta, and F. Trejo, “Modeling of hydrotreating catalyst deactivation for heavy oil hydrocarbons,” *Fuel*, vol. 225, pp. 118–133, 2018, doi: https://doi.org/10.1016/j.fuel.2018.02.085.

[38] L. Chen, Z. Yu, Z. Zong, Z. Zhu, and Q. Wu, “The Effects of Temperature and Hydrogen Partial Pressure on Hydrocracking of Phenanthrene,” *Int. J. Chem.*, vol. 3, Jun. 2011, doi: 10.5539/ijc.v3n2p67.

[39] P. Kokayeff, S. Zink, and P. Roxas, “Hydrotreating in Petroleum Processing,” 2015, pp. 361–434.

[40] W. Joseph, “Three-phase catalytic reactors for hydrogenation and oxidation reactions,” *Phys. Sci. Rev.*, vol. 1, no. 1, 2016, doi: doi:10.1515/psr-2015-0019.

[41] M. Mapiour, “Kinetics and effects of H2 partial pressure on hydrotreating of heavy gas oil,” 2009.

[42] D. Sullivan, S. Metro, and P. R. Pujadó, *Handbook of Petroleum Processing*. 2015.

[43] L. de Oliveira, D. Hudebine, D. Guillaume, and J. Verstraete, “A Review of Kinetic Modeling Methodologies for Complex Processes,” *Oil Gas Sci. Technol.*, vol. 71, p. 45, May 2016, doi: 10.2516/ogst/2016011.

[44] J. Bonnardot, “Modélisation cinétique des réactions d’hydrotraitement par regroupement en familles chimiques,” 1998.

[45] C. López-García, M. Roy-Auberger, T. Chapus, and F. Baco, “Analysis and kinetic modeling in ULSD hydrotreating,” *Prepr. Pap. Am. Chem. Soc. Div. Fuel Chem.*, vol. 48, no. 2, pp. 681–682, 2003.

[46] M. A. Baltanas, K. K. Van Raemdonck, G. F. Froment, and S. R. Mohedas, “Fundamental kinetic modeling of hydroisomerization and hydrocracking on noble metal-loaded faujasites. 1. Rate parameters for hydroisomerization,” *Ind.*

Eng. Chem. Res., vol. 28, no. 7, pp. 899–910, Jul. 1989, doi: 10.1021/ie00091a004.

[47] W. Feng, E. Vynckier, and G. F. Froment, "Single event kinetics of catalytic cracking," *Ind. Eng. Chem. Res.*, vol. 32, no. 12, pp. 2997–3005, Dec. 1993, doi: 10.1021/ie00024a007.

[48] M. Proefschrift, C. Technologie, V. Chemische, and T. C. Voorzitter, "Hydrodenitrogenation Kinetics According to Single-Event Methodology," 2016.

[49] J. W. Thybaut and G. B. Marin, "Single-Event MicroKinetics: Catalyst design for complex reaction networks," *J. Catal.*, vol. 308, pp. 352–362, 2013, doi: https://doi.org/10.1016/j.jcat.2013.08.013.

[50] S. W. Benson and J. H. Buss, "Additivity Rules for the Estimation of Molecular Properties. Thermodynamic Properties," *J. Chem. Phys.*, vol. 29, no. 3, pp. 546–572, Sep. 1958, doi: 10.1063/1.1744539.

[51] K. Surla, D. Guillaume, J. Verstraete, and P. Galtier, "Kinetic Modeling using the Single-Event Methodology: Application to the Isomerization of Light Paraffins," *Oil Gas Sci. Technol.*, vol. 66, pp. 343–365, May 2011, doi: 10.2516/ogst/2011119.

[52] C.-Y. Gau and M. A. Stadtherr, "Reliable nonlinear parameter estimation using interval analysis: error-in-variable approach," *Comput. Chem. Eng.*, vol. 24, no. 2, pp. 631–637, 2000, doi: https://doi.org/10.1016/S0098-1354(00)00363-X.

[53] A. T. Jarullah, I. M. Mujtaba, and A. S. Wood, "Kinetic model development and simulation of simultaneous hydrodenitrogenation and hydrodemetallization of crude oil in trickle bed reactor," *Fuel*, vol. 90, no. 6, pp. 2165–2181, 2011, doi: https://doi.org/10.1016/j.fuel.2011.01.025.

[54] J. Milstein, "The Inverse Problem: Estimation of Kinetic Parameters BT - Modelling of Chemical Reaction Systems," 1981, pp. 92–101.

[55] A. Ruszczyński, *Nonlinear Optimization*. Princeton University Press, 2006.

[56] L. Palagi, "Global optimization issues in deep network regression: an overview," *J. Glob. Optim.*, vol. 73, no. 2, pp. 239–277, 2019, doi: 10.1007/s10898-018-0701-

7.

[57] L. A. Alcázar and J. Ancheyta, “Sensitivity analysis based methodology to estimate the best set of parameters for heterogeneous kinetic models,” *Chem. Eng. J.*, vol. 128, no. 2, pp. 85–93, 2007, doi: https://doi.org/10.1016/j.cej.2006.10.012.

[58] R. Rubinstein and D. Kroese, “Simulation and the Monte Carlo Method,” in *Simulation and the Monte Carlo Method, 2nd edition, by R.Y. Rubinstein and D.P. Kroese. ISBN 9780470177945. Published by Wiley, 2007, 372 pages.*, vol. 707, 2008, p. John Wiley & Sons.

[59] T. H. Ahmed, *Hydrocarbon phase behavior*. Houston: Gulf Pub. Co., 1989.

[60] R. Chacon, A. Canale, A. Bouza, and Y. Sánchez, “Modeling of a three-phase reactor for bitumen-derived gas oil hydrotreating,” *Brazilian J. Chem. Eng.*, vol. 29, pp. 135–146, Mar. 2012, doi: 10.1590/S0104-66322012000100015.

[61] S. Goto and J. M. Smith, “Trickle-bed reactor performance. Part I. Holdup and mass transfer effects,” *AIChE J.*, vol. 21, no. 4, pp. 706–713, Jul. 1975, doi: https://doi.org/10.1002/aic.690210410.

[62] B. E. Reid, R C, Prausnitz, J M, & Poling, *The properties of gases and liquids*, 4th ed. United States, 1975.

[63] D. W. Green and R. H. Perry, *Perry’s Chemical Engineers’ Handbook*, 8th ed. New York: McGraw-Hill Education, 1984.

[64] P. Ghosh, A. T. Andrews, R. J. Quann, and T. R. Halbert, “Detailed Kinetic Model for the Hydro-desulfurization of FCC Naphtha,” *Energy & Fuels*, vol. 23, no. 12, pp. 5743–5759, Dec. 2009, doi: 10.1021/ef900632v.

[65] G. F. Froment, G. A. Depauw, and V. Vanrysselberghe, “Kinetic Modeling and Reactor Simulation in Hydrodesulfurization of Oil Fractions,” *Ind. Eng. Chem. Res.*, vol. 33, no. 12, pp. 2975–2988, Dec. 1994, doi: 10.1021/ie00036a012.

[66] F. Gao and L. Han, “Implementing the Nelder-Mead simplex algorithm with adaptive parameters,” *Comput. Optim. Appl.*, vol. 51, no. 1, pp. 259–277,

2012, doi: 10.1007/s10589-010-9329-3.

[67] J. A. Nelder and R. Mead, “A Simplex Method for Function Minimization,” *Comput. J.*, vol. 7, no. 4, pp. 308–313, Jan. 1965, doi: 10.1093/comjnl/7.4.308.

FACULTY OF ENGINEERING AND ARCHITECTURE

A kinetic study on the desulfurization and denitrogenation of medium oil cuts

Luis Miguel García Riesco

Supervisors: Prof. Dr. Ir. Joris W. Thybaut, Prof. Dr. Ir. Kevin Van Geem.
Counsellors: MSc. Ir. César Pernalete

Master's dissertation submitted in order to obtain the academic degree of
Master of Science in Chemical Engineering

Department of Materials, Textiles and Chemical Engineering
Faculty of Engineering and Architecture
Academic year 2020-2021

GHENT UNIVERSITY